



Measurement of CP asymmetry in $B_s^0 \rightarrow D_s^\mp K^\pm$ decays

LHCb collaboration[†]

Abstract

A measurement of the CP -violating parameters in $B_s^0 \rightarrow D_s^\mp K^\pm$ decays is reported, based on the analysis of proton-proton collision data collected by the LHCb experiment corresponding to an integrated luminosity of 6 fb^{-1} at a centre-of-mass energy of 13 TeV. The measured parameters are $C_f = 0.791 \pm 0.061 \pm 0.022$, $A_f^{\Delta\Gamma} = -0.051 \pm 0.134 \pm 0.058$, $A_{\bar{f}}^{\Delta\Gamma} = -0.303 \pm 0.125 \pm 0.055$, $S_f = -0.571 \pm 0.084 \pm 0.023$ and $S_{\bar{f}} = -0.503 \pm 0.084 \pm 0.025$, where the first uncertainty is statistical and the second systematic. Together with the value of the B_s^0 mixing phase $-2\beta_s$, these parameters are used to obtain a measurement of the CKM angle γ equal to $(74 \pm 12)^\circ$ modulo 180° , where the uncertainty contains both statistical and systematic contributions. This result is combined with the previous LHCb measurement in this channel using 3 fb^{-1} resulting in a determination of $\gamma = (81_{-11}^{+12})^\circ$.

Submitted to JHEP

© 2025 CERN for the benefit of the LHCb collaboration. CC BY 4.0 licence.

[†]Authors are listed at the end of this paper.

1 Introduction

Measurements of the CP asymmetries in $B_{(s)}^0 \rightarrow D_{(s)}^{(*)\mp} h^\pm$ decays,¹ where $h = \pi$ or K , have been performed by the LHCb [1,2], BaBar [3,4] and Belle [5,6] collaborations. These measurements are of particular interest as they constrain elements of the CKM quark-mixing matrix, in which all Standard Model (SM) CP -violation effects arise from a single complex phase [7,8]. The unitarity constraint of the CKM matrix, relevant to the $b \rightarrow u$ and $b \rightarrow c$ transitions in the above decays, can be written as $V_{ud}V_{ub}^* + V_{cd}V_{cb}^* + V_{td}V_{tb}^* = 0$, where V_{ij} are the matrix elements. This constraint can be represented as a triangle in a complex plane in which the internal angle γ is defined by $\gamma = \phi_3 \equiv \arg(-V_{ud}V_{ub}^*/V_{cd}V_{cb}^*)$ and can be probed both indirectly, under the assumption of unitarity, and directly in tree-level processes [9–11]. The consistency between these determinations provides a powerful validation of the SM picture of CP violation. The most accurate determination of the angle γ in tree-level processes is currently obtained by combining LHCb measurements of B^+ , B^0 and B_s^0 decays to final states with a $D_{(s)}$ meson and one or more light mesons. Results from both time-integrated and time-dependent analyses are used, as well as constraints from charm-meson decays [12].

The decay-time-dependent analyses of $B_s^0 \rightarrow D_s^\mp K^\pm$ and $B^0 \rightarrow D^{(*)\mp} \pi^\pm$ tree-level decays are sensitive to the angle γ in the interference of mixing and decay amplitudes [13–18], which for the $B_s^0 \rightarrow D_s^\mp K^\pm$ decay proceed through the leading-order Feynman diagrams shown in Fig. 1. In these decays, the CP -violating parameters are functions of a combination of the angle γ and the relevant mixing phase $\beta_{(s)}$, namely $\gamma + 2\beta$ ($\beta = \phi_1 \equiv \arg(-V_{cd}V_{cb}^*/V_{td}V_{tb}^*)$) in the B^0 system and $\gamma - 2\beta_s$ ($\beta_s \equiv \arg(-V_{ts}V_{tb}^*/V_{cs}V_{cb}^*)$) in the B_s^0 system. In $B^0 \rightarrow D^{(*)\mp} \pi^\pm$ decays the ratio between the interfering decay amplitudes is small, $r_{D^{(*)}\pi} = |A(\bar{B}^0 \rightarrow D^{(*)-} \pi^+)/A(B^0 \rightarrow D^{(*)-} \pi^+)| \approx 0.02$, which limits the sensitivity to the CKM angle γ [19]. By contrast, the ratio is larger for $B_s^0 \rightarrow D_s^- K^+$ decays, $r_{D_s K} = |A(\bar{B}_s^0 \rightarrow D_s^- K^+)/A(B_s^0 \rightarrow D_s^- K^+)| \approx 0.4$, since both $b \rightarrow cs\bar{u}$ and $b \rightarrow u\bar{c}s$ amplitudes have similar magnitudes, of $\mathcal{O}(\lambda^3)$, where $\lambda \approx 0.23$ is the sine of the Cabibbo angle [20,21].

This paper presents a measurement of the CP -violating parameters in $B_s^0 \rightarrow D_s^\mp K^\pm$ decays using a data set of proton-proton (pp) collisions recorded with the LHCb detector at a centre-of-mass energy $\sqrt{s} = 13$ TeV during the Run 2 data-taking period of the LHC (2015–2018). This data set corresponds to an integrated luminosity of 6 fb^{-1} . The decays of the D_s^- meson into the final states $K^-\pi^+\pi^-$, $\pi^-\pi^+\pi^-$ and $K^-K^+\pi^-$ are analysed. The analysis strategy is similar to that of Ref. [1], with the selection, fit model and determination of systematic uncertainties reoptimised. These improvements profit from better trigger and reconstruction performances of the LHCb experiment throughout Run 2 [22].

The determination of the CP -violating parameters is achieved using a two-stage fitting procedure. At the first stage, the $B_s^0 \rightarrow D_s^\mp K^\pm$ signal is statistically separated from background components using the $sPlot$ technique, where the signal weights are determined from a two-dimensional fit to the $m(D_s^\mp K^\pm)$ and $m(h^- h^+ h^\mp)$ distributions [23], where h denotes either a kaon or a pion in the different D_s^\mp decays. Each fit component is factorised using the product of the probability density functions (PDFs) modelling the $m(D_s^\mp K^\pm)$ and $m(h^- h^+ h^\mp)$ invariant-mass distributions since their correlations are

¹Inclusion of charge-conjugate modes is implied throughout, except where explicitly stated.

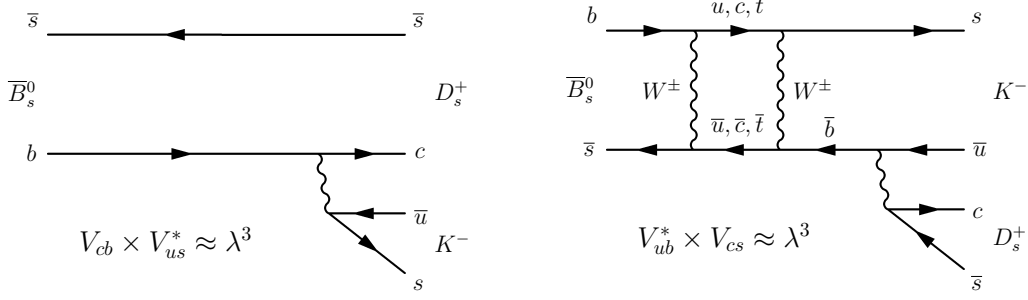


Figure 1: Leading-order Feynman diagrams for $\bar{B}_s^0 \rightarrow D_s^+ K^-$ decays (left) without and (right) with B_s^0 - \bar{B}_s^0 mixing.

determined to be negligible in simulation samples. A systematic uncertainty is assigned to account for the impact of any remaining correlations. The two-dimensional fit is performed simultaneously to all D_s^- final states considered in this analysis and to three data-taking periods (2015–2016, 2017, 2018), where the 2015 sample is fitted together with 2016 data due to its limited size. In the second stage, an unbinned maximum-likelihood fit to the decay-time distribution of the background-subtracted $B_s^0 \rightarrow D_s^\mp K^\pm$ signal is performed to determine the CP -violating parameters. In the decay-time fit the data-taking periods are fitted simultaneously, while the D_s^- final states are combined.

Finally, the results of the present analysis are combined with those of Ref. [1], which uses an integrated luminosity of 3 fb^{-1} recorded at $\sqrt{s} = 7$ and 8 TeV during the Run 1 data-taking period (2011–2012) with the external inputs updated to match the values used in the present analysis.

1.1 Decay rates and CP -violating parameters

Following the conventions of Ref. [1], the time-dependent decay rates of an initially produced flavour eigenstate B_s^0 or \bar{B}_s^0 decaying to final state f can be written as

$$\frac{d\Gamma_{B_s^0 \rightarrow f}(t)}{dt} = \frac{1}{2} |A_f|^2 (1 + |\lambda_f|^2) e^{-\Gamma_s t} \left[\cosh\left(\frac{\Delta\Gamma_s t}{2}\right) + A_f^{\Delta\Gamma} \sinh\left(\frac{\Delta\Gamma_s t}{2}\right) + C_f \cos(\Delta m_s t) - S_f \sin(\Delta m_s t) \right], \quad (1)$$

$$\frac{d\Gamma_{\bar{B}_s^0 \rightarrow f}(t)}{dt} = \frac{1}{2} |A_f|^2 \left| \frac{p}{q} \right|^2 (1 + |\lambda_f|^2) e^{-\Gamma_s t} \left[\cosh\left(\frac{\Delta\Gamma_s t}{2}\right) + A_f^{\Delta\Gamma} \sinh\left(\frac{\Delta\Gamma_s t}{2}\right) - C_f \cos(\Delta m_s t) + S_f \sin(\Delta m_s t) \right], \quad (2)$$

where $\lambda_f \equiv (q/p)(\bar{A}_f/A_f)$, $A_f(\bar{A}_f)$ is the amplitude of a B_s^0 (\bar{B}_s^0) decay to the final state $f \equiv D_s^- K^+$ and the complex coefficients p and q describe the mixing of the light, $|B_L\rangle$, and heavy, $|B_H\rangle$, mass and flavour eigenstates according to

$$|B_L\rangle \equiv p|B_s^0\rangle + q|\bar{B}_s^0\rangle \quad \text{and} \quad |B_H\rangle \equiv p|B_s^0\rangle - q|\bar{B}_s^0\rangle, \quad (3)$$

with the normalisation condition $|p|^2 + |q|^2 = 1$. Here, Γ_s is the B_s^0 decay width or inverse B_s^0 lifetime, $\Delta\Gamma_s \equiv \Gamma_{B_L} - \Gamma_{B_H}$ is the decay-width difference between the light and heavy mass eigenstates and $\Delta m_s \equiv m_{B_H} - m_{B_L}$ is the mixing frequency in the B_s^0 system.

Similar equations can be obtained for decays into the CP -conjugate final state $\bar{f} \equiv D_s^+ K^-$ by replacing C_f by $C_{\bar{f}}$, S_f by $S_{\bar{f}}$, and $A_f^{\Delta\Gamma}$ by $A_{\bar{f}}^{\Delta\Gamma}$. The CP -asymmetry parameters can be written as

$$\begin{aligned} C_f &= \frac{1 - |\lambda_f|^2}{1 + |\lambda_f|^2} = -C_{\bar{f}} = -\frac{1 - |\lambda_{\bar{f}}|^2}{1 + |\lambda_{\bar{f}}|^2}, \\ A_f^{\Delta\Gamma} &= \frac{-2\mathcal{R}e(\lambda_f)}{1 + |\lambda_f|^2}, \quad A_{\bar{f}}^{\Delta\Gamma} = \frac{-2\mathcal{R}e(\lambda_{\bar{f}})}{1 + |\lambda_{\bar{f}}|^2}, \\ S_f &= \frac{2\mathcal{I}m(\lambda_f)}{1 + |\lambda_f|^2}, \quad S_{\bar{f}} = \frac{2\mathcal{I}m(\lambda_{\bar{f}})}{1 + |\lambda_{\bar{f}}|^2}. \end{aligned} \quad (4)$$

The relation $C_f = -C_{\bar{f}}$ results from the conditions $|q/p| = 1$ and $|\lambda_f| = |1/\lambda_{\bar{f}}|$, which imply no CP violation both in mixing, in agreement with current measurements [24], and decay. The second assumption is motivated by the fact that only a single amplitude contributes to each initial-to-final-state transition. Finally, the CP observables are related to the magnitude of the amplitude ratio $r_{D_s K}$, the strong-phase difference δ between the amplitudes $A(\bar{B}_s^0 \rightarrow D_s^- K^+)$ and $A(B_s^0 \rightarrow D_s^- K^+)$ and the weak-phase difference $\gamma - 2\beta_s$ by the following equations

$$\begin{aligned} C_f &= \frac{1 - r_{D_s K}^2}{1 + r_{D_s K}^2}, \\ A_f^{\Delta\Gamma} &= \frac{-2r_{D_s K} \cos(\delta - (\gamma - 2\beta_s))}{1 + r_{D_s K}^2}, \quad A_{\bar{f}}^{\Delta\Gamma} = \frac{-2r_{D_s K} \cos(\delta + (\gamma - 2\beta_s))}{1 + r_{D_s K}^2}, \\ S_f &= \frac{2r_{D_s K} \sin(\delta - (\gamma - 2\beta_s))}{1 + r_{D_s K}^2}, \quad S_{\bar{f}} = \frac{-2r_{D_s K} \sin(\delta + (\gamma - 2\beta_s))}{1 + r_{D_s K}^2}. \end{aligned} \quad (5)$$

These observables are used to extract γ , δ and $r_{D_s K}$ while fixing $-2\beta_s$, as discussed in Sec. 7. The combined Run 1 and Run 2 result is also expressed in terms of $\gamma - 2\beta_s$. This combined quantity offers complementary sensitivity on a potential new physics phase in B_s^0 - \bar{B}_s^0 mixing.

2 Detector and software

The LHCb detector [25, 26] is a single-arm forward spectrometer covering the pseudorapidity range $2 < \eta < 5$, designed for the study of particles containing b or c quarks. The detector includes a high-precision tracking system consisting of a silicon-strip vertex detector surrounding the pp interaction region, a large-area silicon-strip detector located upstream of a dipole magnet with a bending power of about 4 T m, and three stations of silicon-strip detectors and straw drift tubes placed downstream of the magnet. The tracking system provides a measurement of the momentum, p , of charged particles with a relative uncertainty that varies from 0.5% at low momentum to 1.0% at 200 GeV/ c . The minimum distance of a track to a primary pp collision vertex (PV), the impact parameter (IP), is measured with a resolution of $(15 + 29/p_T) \mu\text{m}$, where p_T is the component of the momentum transverse to the beam, in GeV/ c . Different types of charged hadrons are distinguished using information from two ring-imaging Cherenkov detectors. Photons, electrons and hadrons are identified by a calorimeter system consisting of scintillating-pad and preshower detectors, an electromagnetic and a hadronic

calorimeter. Muons are identified by a system composed of alternating layers of iron and multiwire proportional chambers. The online event selection is performed by a trigger, which consists of a hardware stage, based on information from the calorimeter and muon systems, followed by a software stage, which applies a full event reconstruction.

At the hardware trigger stage, events are required to have a muon with high p_T or a hadron, photon or electron with high transverse energy in the calorimeters. The software trigger requires a two-, three- or four-track secondary vertex with a significant displacement from any primary pp interaction vertex. At least one charged particle must have a transverse momentum $p_T > 1.6 \text{ GeV}/c$ and be inconsistent with originating from a PV. A multivariate algorithm [27, 28] is used for the identification of secondary vertices consistent with the decay of a b hadron.

Simulation is required to model the effects of the detector acceptance and the imposed selection requirements. In the simulation, pp collisions are generated using PYTHIA [29] with a specific LHCb configuration [30]. Decays of unstable particles are described by EVTGEN [31], in which final-state radiation is generated using PHOTOS [32]. The interaction of the generated particles with the detector, and its response, are implemented using the GEANT4 toolkit [33] as described in Ref. [34].

3 Candidate selection

The selection criteria are similar to those used in Ref. [1], but updated to reflect improvements in reconstruction performance. Samples of signal $B_s^0 \rightarrow D_s^\mp K^\pm$ and two control channels $B_s^0 \rightarrow D_s^- \pi^+$ and $B^0 \rightarrow D^- \pi^+$ decays are selected by combining a $D_{(s)}^-$ candidate with a particle, referred to as ‘‘companion’’ in the following, consistent with the hypothesis of being either a kaon or a pion. The D^- meson is reconstructed using the $D^- \rightarrow K^+ \pi^- \pi^-$ decay. The D_s^- meson is reconstructed using the final states $K^- \pi^+ \pi^-$, $\pi^- \pi^+ \pi^-$ and $K^- K^+ \pi^-$, with the latter further subdivided into $D_s^- \rightarrow \phi \pi^-$, $D_s^- \rightarrow K^*(892)^0 K^-$, and the remaining regions of the phase space denoted as the nonresonant $D_s^- \rightarrow (K^- K^+ \pi^-)_{\text{NR}}$ component. The separation between these five decay modes is based on kinematic and particle identification (PID) requirements, allowing for the optimisation of the signal selection while accounting for the different background contributions in each sample. Furthermore, each decay mode undergoes a combination of PID and kinematic vetoes to suppress cross-feed backgrounds from $B^0 \rightarrow D^- h^+$ or $\bar{A}_b^0 \rightarrow \bar{A}_c^- h^+$ decays, as well as background contributions containing J/ψ , D^0 and K^{*0} decays. The distinction between $B_s^0 \rightarrow D_s^- \pi^+$ and $B_s^0 \rightarrow D_s^\mp K^\pm$ decays is achieved with mutually exclusive requirements on the PID information of the companion track.

The B_s^0 candidate is associated with the PV with the smallest impact parameter χ^2 , calculated as the difference in χ^2 for the vertex fit of the PV with and without the considered particle (χ_{IP}^2). The decay-time resolution of the B_s^0 candidate is enhanced through a kinematic fit [35], which constrains the candidate to originate from the associated PV. Similarly, the measured values of the $D_s^\mp K^\pm$ invariant mass are obtained by constraining the D_s^- invariant mass to the world-average value [21]. The B_s^0 and D_s^- candidates are required to have invariant masses within $[5300, 5800] \text{ MeV}/c^2$ and $[1930, 2015] \text{ MeV}/c^2$, respectively.

Contributions from b -hadron decays that do not include a charm hadron are suppressed by imposing a D_s^- flight-distance significance requirement. This quantity is defined as the

distance between the B_s^0 and D_s^- decay vertices divided by its uncertainty.

To suppress combinatorial background due to random track combinations, a gradient-boosted decision tree (BDTG) algorithm [36, 37] is employed. The BDTG classifier is trained using the $B_s^0 \rightarrow D_s^- \pi^+$ control sample reconstructed in the $D_s^- \rightarrow K^- K^+ \pi^-$ final state, as detailed in Ref. [38]. Since all channels in this analysis exhibit similar kinematics and no PID information is used in the BDTG classifier, the resulting BDTG algorithm performs equally well on other D_s^- decay modes. The classifier uses several track-related variables, including the transverse momentum of the companion particle, the radial flight distance of both the b - and c -hadron candidates and the companion and b -hadron's minimum χ_{IP}^2 . A detailed description can be found elsewhere [1, 39]. Fewer than 0.5% of the events passing the selection requirements contain more than one signal candidate, and in such cases, all candidates are used in the analysis.

4 Two-dimensional invariant-mass fit

The selected $B_s^0 \rightarrow D_s^\mp K^\pm$ candidates are fitted using a two-dimensional unbinned extended maximum-likelihood fit to the $m(D_s^\mp K^\pm)$ and $m(h^- h^+ h^\mp)$ distributions, in order to statistically remove background components using the *sPlot* technique [23] in the subsequent decay-time fit.

The signal and background PDFs for the invariant-mass fit are derived from the simulated samples after being corrected to better reproduce data. Specifically, the $B^0 \rightarrow D^- \pi^+$ control mode is used to correct for differences between simulation and data in the distributions of the B_s^0 and D_s^- vertices' uncertainty on the z -position and to correct for a shift between data and simulation in the $m(D_s^\mp K^\pm)$ invariant mass. The PID distributions in the simulation are corrected to match those in data using $D^{*+} \rightarrow D^0 \pi^+$ and $\Lambda^0 \rightarrow p \pi^-$ calibration samples. More information about this procedure is provided in Ref. [40].

The shape of the $m(D_s^\mp K^\pm)$ distribution for signal candidates is modelled using the sum of a double-sided Hypatia function [41] and a Johnson S_U function [42], sharing a common peak position. This combination effectively describes the main peak and the radiative tail. The signal PDFs are separately derived from simulated $B_s^0 \rightarrow D_s^\mp K^\pm$ candidates for each D_s^- decay mode and data-taking period. The signal shapes are fixed in the data fit with two exceptions. Separate peak parameters are used for the three data-taking periods, which are left free in the fit. Furthermore, the widths of the Hypatia functions are fixed to the values determined from simulation, while the widths of the Johnson S_U functions are left free. This adjustment compensates for mass-resolution differences between simulation and data.

The $m(h^- h^+ h^\mp)$ signal distribution is also described using the combination of a double-sided Hypatia function and a Johnson S_U function, sharing a common peak position. The signal PDFs are derived from simulation for each D_s^- decay mode and data-taking period. Similar to the $m(D_s^\mp K^\pm)$ invariant-mass parameterisation, only the common peak position and the width of the Johnson S_U function are free parameters in the fit to data.

The combinatorial background comprises random track combinations that do not originate from D_s^- meson decay, as well as backgrounds containing a true D_s^- decay combined with a random companion track. The functional form of the combinatorial background is motivated by the upper $m(D_s^\mp K^\pm)$ invariant-mass sidebands, [5600, 6800] MeV/ c^2 , with

all parameters allowed to vary in the two-dimensional fit. It is parameterised separately for each D_s^- decay mode and each period of data taking: an exponential plus constant is found to be optimal to describe the combinatorial background component for the $D_s^- \rightarrow K^- K^+ \pi^-$ decay modes, while for the $D_s^- \rightarrow K^- \pi^+ \pi^-$ and $D_s^- \rightarrow \pi^- \pi^+ \pi^-$ final states a single exponential is found to be sufficient. The combinatorial component in the $m(h^- h^+ h^\mp)$ distribution is described by the sum of an exponential and the D_s^- signal shape, where the peak position is shared with the signal itself, modelling the contributions from random track combinations and true D_s^- mesons paired with a random track, respectively. The exponent and the fraction between the exponential and the signal shape are free to vary in the fit to data.

In the two-dimensional fit, besides the signal and the combinatorial background, the following background contributions are considered: fully reconstructed $B^0 \rightarrow D_s^- K^+$ decays, companion-track misidentified $B_s^0 \rightarrow D_s^- \pi^+$ and $\Lambda_b^0 \rightarrow D_s^- p$ decays, companion-track misidentified partially reconstructed $B_s^0 \rightarrow D_s^{*-} \pi^+$, $B_s^0 \rightarrow D_s^- \rho^+$ and $\Lambda_b^0 \rightarrow D_s^{*-} p$ decays, where the neutral γ or π^0 from $D_s^{*-} \rightarrow D_s^- \gamma / \pi^0$ and $\rho^+ \rightarrow \pi^+ \pi^0$ is not reconstructed. Furthermore, the $B^0 \rightarrow D^- K^+$, $B^0 \rightarrow D^- \pi^+$, $\bar{\Lambda}_b^0 \rightarrow \bar{\Lambda}_c^- K^+$ and $\bar{\Lambda}_b^0 \rightarrow \bar{\Lambda}_c^- \pi^+$ components are included, where a misidentified final state causes the c -hadron to be reconstructed as a D_s^- meson.

In the fit to the $m(D_s^\mp K^\pm)$ distribution, double-sided Hypatia functions are used for the fully reconstructed $B^0 \rightarrow D_s^- K^+$ and the partially reconstructed $B_s^0 \rightarrow D_s^{*-} \pi^+$ contributions, the sum of a double-sided Hypatia and a Johnson S_U function is used to describe the $B_s^0 \rightarrow D_s^- \pi^+$ decays, the contribution from partially reconstructed $B_s^0 \rightarrow D_s^- \rho^+$ decays is modelled using the sum of two exponential functions. For the $m(D_s^\mp K^\pm)$ distribution of the remaining partially or fully reconstructed backgrounds, the shapes of the distributions in the simulation are defined using a nonparametric kernel estimation method [43], corrected to match the PID efficiency and kinematic distributions observed in the data. In the fit to the $m(h^- h^+ h^\mp)$ distribution, the signal shape is used for the $B^0 \rightarrow D_s^- K^+$, $B_s^0 \rightarrow D_s^- \pi^+$, $B_s^0 \rightarrow D_s^{*-} \pi^+$, $B_s^0 \rightarrow D_s^- \rho^+$, $\Lambda_b^0 \rightarrow D_s^- p$ and $\Lambda_b^0 \rightarrow D_s^{*-} p$ contributions, whereas the other background components are described using a nonparametric kernel estimation method.

The invariant-mass fit is performed simultaneously across the different D_s^- decay modes and periods of data taking. For each D_s^- decay mode, the PDF is constructed from the sum of signal and background contributions. Most background yields are allowed to vary freely in the fit, except for those with an expected contribution below 2% of the signal yield, specifically: $B^0 \rightarrow D^- K^+$, $B^0 \rightarrow D^- \pi^+$, $\bar{\Lambda}_b^0 \rightarrow \bar{\Lambda}_c^- K^+$ and $\bar{\Lambda}_b^0 \rightarrow \bar{\Lambda}_c^- \pi^+$. In such cases, the yields are fixed to the results of dedicated fits to $B^0 \rightarrow D^- \pi^+$ and $\bar{\Lambda}_b^0 \rightarrow \bar{\Lambda}_c^- \pi^+$ candidates, corrected by the known branching fractions and selection efficiencies relative to the selection of the $B_s^0 \rightarrow D_s^\mp K^\pm$ candidates [21].

The $D_s^\mp K^\pm$ and $h^\mp h^+ h^-$ invariant-mass distributions, summed over the D_s^- decay modes and the data-taking periods, are shown in Fig. 2 with the results of the fit overlaid. The signal yield, confirmed to be unbiased through data-like pseudoexperiments, is determined to be $20\,949 \pm 180$, where the uncertainty is statistical only. The invariant-mass fit to the $B_s^0 \rightarrow D_s^- \pi^+$ control mode is reported in Ref. [38].

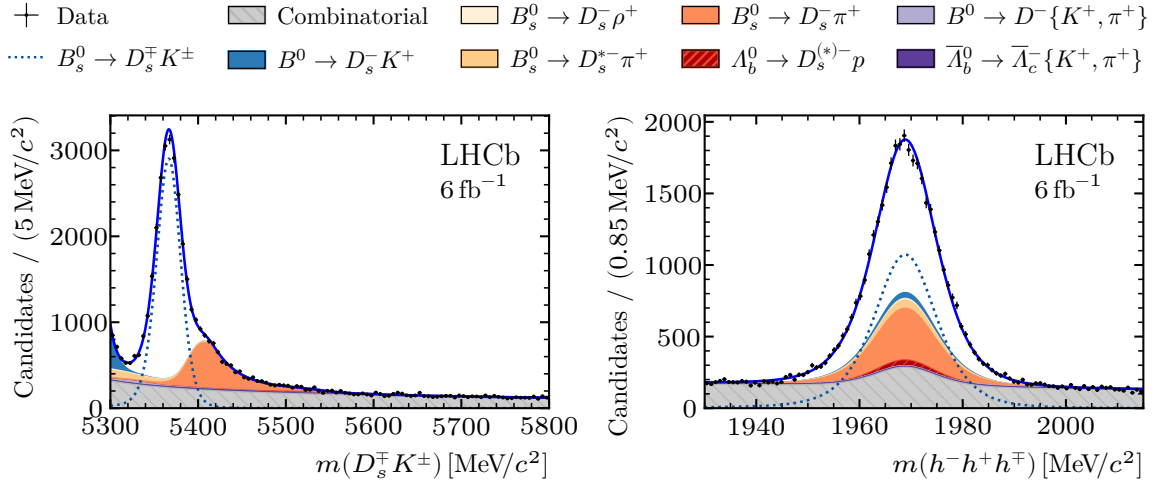


Figure 2: Distributions of the (left) $D_s^\mp K^\pm$ and (right) $h^- h^+ h^\mp$ invariant masses for selected $D_s^\mp K^\pm$ candidates. The contributions from all D_s^- decay modes and years of data taking are combined. The solid-blue curve is the total result of the two-dimensional fit. The dotted curve shows the $B_s^0 \rightarrow D_s^\mp K^\pm$ signal and the shaded-stacked histograms show the different background contributions.

5 Decay-time fit

The goal of the decay-time fit is to determine the CP -violating parameters C_f , S_f , $S_{\bar{f}}$, $A_f^{\Delta\Gamma}$ and $A_{\bar{f}}^{\Delta\Gamma}$ from the decay-time distribution of $B_s^0 \rightarrow D_s^\mp K^\pm$ decays which follow a PDF obtained from Eqs. 1 and 2. The decay-time distribution of the signal candidates in the reconstructed $B_s^0 \rightarrow D_s^\mp K^\pm$ decays is obtained using the *sPlot* technique following the two-dimensional mass fit. Several experimental effects are accounted for in the fit to describe the observed decay rates, such as the decay-time resolution and acceptance and the performance of the flavour-tagging algorithms to determine the initial B_s^0 flavour.

To account for the decay-time resolution, the signal PDF is convolved with a Gaussian function whose width, σ_t , is evaluated for each candidate based on the decay-time uncertainty estimated by the vertex fit, δ_t . The decay-time resolution model is calibrated using a control sample of artificial $B_s^0 \rightarrow D_s^\mp K^\pm$ decays obtained by combining a D_s^- meson originating promptly from the pp interaction point with an oppositely charged companion meson coming from the same origin. The selection requirements are the same as for the signal, except for those that depend on the displacement from the pp collision point. These B_s^0 candidates have a decay vertex compatible with a lifetime of zero, up to resolution and alignment effects, thus their decay-time distribution determines the decay-time resolution. The sample of prompt D_s^- candidates is divided into ten equally populated bins of decay-time uncertainty. In each subsample, the decay-time resolution is determined from a fit to the decay-time distribution. The resulting decay-time resolutions as a function of decay-time uncertainty are then fitted with a linear function, $\sigma_t = p_0 + p_1 \cdot \delta_t$. The resulting average decay-time resolution is about 46 fs.

A bias in the measured B_s^0 decay time, originating from residual detector misalignment, has been identified in the analysis of $B_s^0 \rightarrow D_s^- \pi^+$ decays for the Δm_s measurement [38]. This bias was determined from the analysis of the same calibration sample of prompt D_s^-

mesons used for the study of the aforementioned decay-time resolution model. Corrections for the differences between the prompt D_s^- and signal samples were obtained using intentionally misaligned simulated samples. This measurement takes the bias obtained in the Δm_s measurement with a correction to account for differences in selection criteria between the two analyses. The decay-time bias, determined for each period of data taking, is corrected for in the decay-time fit and amounts to about -3 fs.

The initial flavour of the B_s^0 meson is needed to determine its contribution to the corresponding decay rate. This information is provided by flavour-tagging algorithms which exploit different processes correlated with the b -hadron production in pp collisions. Beauty quarks are predominantly produced through $b\bar{b}$ pairs. While one of these b quarks leads to the signal B_s^0 meson, the other leads to a b hadron that decays independently. The decay chain of the other b hadron is exploited by the opposite-side (OS) tagging algorithms [44] to determine the initial flavour of the signal B_s^0 meson. The OS muon and OS electron taggers exploit the semileptonic decay of the b hadron, and the OS kaon and the OS charm taggers identify remnants from $b \rightarrow c \rightarrow s$ and $b \rightarrow c$ transitions, respectively. Furthermore, the OS vertex-charge tagger reconstructs an effective charge of a displaced vertex from the OS b -hadron decay [45]. Each of these algorithms infers the initial B_s^0 meson flavour from the charge of either a reconstructed tagging particle or, in the case of the OS vertex tagger, of a reconstructed vertex. Additionally, the same-side (SS) kaon tagger determines the initial flavour of the B_s^0 signal from the charge of kaons originating from the $s\bar{s}$ pair produced in the fragmentation process that leads to the signal B_s^0 meson [46]. In addition to the tag decision, representing the determined flavour, the algorithms provide an estimate of the probability that the decision is wrong, the estimated mistag probability, η . This estimate does not necessarily match the correct mistag probability, ω , of the data sample. Hence, a calibration is performed using a control sample of flavour-specific $B_s^0 \rightarrow D_s^- \pi^+$ decays to provide the measured mistag following the procedure described in Ref. [38]. The calibration functions are defined as

$$\omega^{\text{tag},y}(\eta^{\text{tag},y}) = \sum_{i=0}^1 \left(f_i^{\text{tag},y} + \frac{1}{2} \Delta f_i^{\text{tag},y} \right) \cdot (\eta^{\text{tag},y} - \langle \eta \rangle^{\text{tag},y})^i \quad \text{for } B_s^0, \quad (6)$$

$$\text{and} \quad \bar{\omega}^{\text{tag},y}(\eta^{\text{tag},y}) = \sum_{i=0}^1 \left(f_i^{\text{tag},y} - \frac{1}{2} \Delta f_i^{\text{tag},y} \right) \cdot (\eta^{\text{tag},y} - \langle \eta \rangle^{\text{tag},y})^i \quad \text{for } \bar{B}_s^0, \quad (7)$$

where $\langle \eta \rangle^{\text{tag},y}$ is the average mistag probability, index i identifies each of the two flavour-tagging calibration parameters $f_i^{\text{tag},y}$. The parameters $\Delta f_i^{\text{tag},y}$ are introduced to allow for different calibrations for B_s^0 and \bar{B}_s^0 candidates. Each tagger (tag = OS, SS) is independently calibrated on each data sample y (2015–2016, 2017, 2018).

The tagging information is included in the PDF used in the decay-time fit, for which the tagging decision assigns candidates to the corresponding decay rate described by Eqs. 1 and 2. The mistag probability causes a reduction of the oscillation amplitude by a dilution factor $D = (1 - 2\omega)$. In the fit, the calibration is performed by constraining the function of the predicted mistag described by Eqs. 6 and 7. Only two taggers are constrained in the fit: the SS kaon tagger and the OS combination, where the individual tag decisions and mistag estimates of all OS taggers are combined into a single decision and mistag estimate.

The tagging efficiency of the full sample is $\varepsilon = (80.30 \pm 0.07)\%$ with an average mistag fraction of $\omega = (36.21 \pm 0.02 \pm 0.17)\%$, where the first uncertainty is due to the finite

size of the calibration sample and the second is due to the uncertainty of the calibration parameters. This results in a tagging power of $(6.10 \pm 0.02 \pm 0.15)\%$, which indicates the remaining statistical power of the flavour-tagged sample, relative to a perfectly tagged sample. For comparison, the tagging power achieved in Run 1 was $(5.80 \pm 0.25)\%$ [1].

Since the CP -violating parameters depend on the decay-time acceptance, the latter needs to be determined. For flavour-specific $B_s^0 \rightarrow D_s^- \pi^+$ decays, where $C_f = -C_{\bar{f}} = 1$ and $S_f = S_{\bar{f}} = 0$, the decay-time acceptance can be determined from a fit to the decay-time distribution with Γ_s and $\Delta\Gamma_s$ parameters fixed to the combination of LHCb results [47]. In the $B_s^0 \rightarrow D_s^\mp K^\pm$ fit, the decay-time acceptance is fixed to the result obtained from the $B_s^0 \rightarrow D_s^- \pi^+$ data fit, corrected by the decay-time acceptance ratio of the two modes estimated from simulation, which is weighted to match the data as described in Sec. 4. The decay-time acceptance is modelled using segments of cubic B-splines, which are implemented analytically in the decay-time fit [48]. The spline boundaries, also known as knots, are chosen in order to accurately model the features of the decay-time acceptance shape. The signal decay-time PDF is then adjusted by multiplying by the decay-time acceptance model.

The decay-time fit requires additional inputs in the form of the following parameters

$$\begin{aligned}
\Delta m_s &= (17.7683 \pm 0.0057) \text{ ps}^{-1} , \\
\Gamma_s &= (0.6563 \pm 0.0020) \text{ ps}^{-1} , \\
\Delta\Gamma_s &= (0.085 \pm 0.004) \text{ ps}^{-1} , \\
A_{\text{prod}} &= (-0.33 \pm 0.32)\% , \\
A_{\text{det}} &= (0.96 \pm 0.15)\% ,
\end{aligned} \tag{8}$$

which are fixed to their central values in the baseline decay-time fit and varied within their uncertainties to determine the associated systematic uncertainties. The values of Δm_s , Γ_s and $\Delta\Gamma_s$ are based on LHCb measurements [38, 47]. The production asymmetry, A_{prod} , is fixed to the value obtained in Ref. [38] and is defined as the relative difference in the B_s^0 and \bar{B}_s^0 production cross-section. The parameter A_{det} is defined as the relative difference in detection efficiencies between the $D_s^- K^+$ and the $D_s^+ K^-$ final states. This is evaluated following the method described in Ref. [49], where the detection asymmetry is evaluated for $K^+ \pi^-$ pairs using $D^+ \rightarrow K^- \pi^+ \pi^+$ and $D^+ \rightarrow \bar{K}^0 \pi^+$ decays. For this measurement, an average asymmetry over the D_s^- final states is calculated using the signal yields obtained from the invariant-mass fit. Its value is compatible with the $K^+ \pi^-$ -pair detection asymmetry in Ref. [50], where the asymmetry was evaluated for $B^+ \rightarrow D \pi^+$ decays. The detection and the production asymmetries contribute to the decay-time PDF with multiplicative factors of $(1 \pm A_{\text{prod}})$ and $(1 \pm A_{\text{det}})$ to the decay rates defined by Eqs. 1 and 2, depending on the tagged initial state and the reconstructed final state.

The CP -violating parameters are determined in a weighted maximum-likelihood fit to the flavour-tagged decay-time distributions. The fit is performed simultaneously to all five D_s^- final states and three data-taking periods, where calibrations of the decay-time resolution and the mistag probability are constrained individually for each data-taking period. The fitted covariance matrix is corrected following an asymptotically correct approach described in Ref. [51] to provide good coverage of the uncertainties following the use of the *sPlot* method. The resulting CP -violating parameters are listed in Table 1 and the corresponding statistical correlation matrix is given in Table 2.

The decay-time distribution and mixing asymmetry of the $D_s^- K^+$ and $D_s^+ K^-$ final

Table 1: Values of the CP -violating parameters obtained from the decay-time fit to $B_s^0 \rightarrow D_s^\mp K^\pm$ candidates. The first uncertainty is statistical and the second is systematic.

Parameter	Value
C_f	$0.791 \pm 0.061 \pm 0.022$
$A_f^{\Delta\Gamma}$	$-0.051 \pm 0.134 \pm 0.058$
$A_{\bar{f}}^{\Delta\Gamma}$	$-0.303 \pm 0.125 \pm 0.055$
S_f	$-0.571 \pm 0.084 \pm 0.023$
$S_{\bar{f}}$	$-0.503 \pm 0.084 \pm 0.025$

Table 2: Statistical correlation matrix of the CP observables. Other fit parameters have negligible correlations with the CP observables.

Parameter	C_f	$A_f^{\Delta\Gamma}$	$A_{\bar{f}}^{\Delta\Gamma}$	S_f	$S_{\bar{f}}$
C_f	1	0.134	0.130	0.039	0.022
$A_f^{\Delta\Gamma}$		1	0.501	-0.108	-0.036
$A_{\bar{f}}^{\Delta\Gamma}$			1	-0.056	-0.067
S_f				1	0.006
$S_{\bar{f}}$					1

states summed over all data-taking periods is shown in Fig. 3, where the fit result is overlaid. The mixing asymmetry is defined as the relative difference between events flavour-tagged as B_s^0 and \bar{B}_s^0 , decaying to the $D_s^- K^+$ or $D_s^+ K^-$ final state as a function of decay time. The CP observables are represented in the $(\mathcal{R}e[2\lambda_f/(1+|\lambda_f|^2)], \mathcal{I}m[2\lambda_f/(1+|\lambda_f|^2)])$ Cartesian plane in Fig. 4. The agreement of the $(-A_f^{\Delta\Gamma}, S_f)$ and $(-A_{\bar{f}}^{\Delta\Gamma}, S_{\bar{f}})$ contours with the $\sqrt{1-C_f^2}$ band indicates that the results are in good agreement with the constraint $C_f^2 + S_f^2 + A_f^{\Delta\Gamma^2} = 1$ that relates to Eq. 5. Using the statistical and systematic uncertainties reported in Table 1 and the corresponding correlations, CP violation in the interference of mixing and decay, *i.e.* $S_f \neq -S_{\bar{f}}$, is observed with a significance of 8.6σ . The dependence of the CP observables on the values of the Γ_s , $\Delta\Gamma_s$ and Δm_s parameters is provided in Appendix A.

6 Systematic uncertainties

Systematic uncertainties are evaluated due to various factors such as the modelling of the invariant-mass fit, fixed parameters in the decay-time fit, namely those in Eq. 8, and the limited knowledge of the decay-time resolution and acceptance. Additionally, the effect of ignoring correlations among observables is assessed. Table 3 summarises the various contributions to the systematic uncertainty, which are described below.

The systematic uncertainty due to fixed parameters in the invariant-mass fit is determined by repeating fits to the data, in which the fixed parameters for signal and background shapes are varied by ± 1 standard deviation. Additionally, fixed background yields and relative fractions among background components are varied. For each parame-

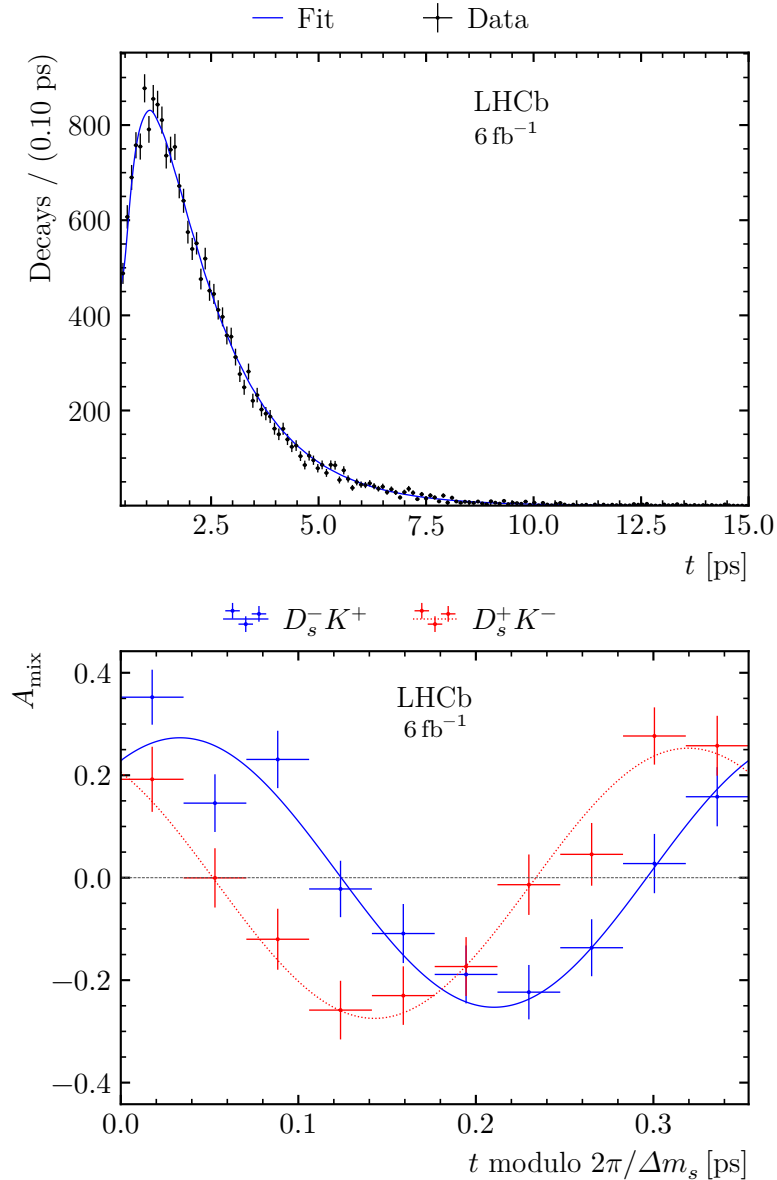


Figure 3: (Top) Decay-time distribution of $B_s^0 \rightarrow D_s^\mp K^\pm$ signal candidates, where the background is statistically subtracted using the *sPlot* technique. (Bottom) Mixing asymmetry, A_{mix} , for the (blue) $D_s^- K^+$ and the (red) $D_s^+ K^-$ final states, folded into one mixing period, $2\pi/\Delta m_s$. In both plots, the curves show the result of the decay-time fit.

ter, the average difference of the CP observables between the baseline and the modified fit is taken as the systematic uncertainty. After evaluating single contributions, all sources are added in quadrature.

The flavour-tagging parameters are constrained to the values found in the $B_s^0 \rightarrow D_s^- \pi^+$ decay-time fit. Systematic uncertainties are assigned by performing a single $B_s^0 \rightarrow D_s^\mp K^\pm$ decay-time fit, where the uncertainties on the flavour-tagging parameters are enlarged to account for their systematic effects. This fit accounts for both the variation of the fit strategy used in the $B_s^0 \rightarrow D_s^- \pi^+$ data fit, as described in Ref. [38], and the portability of the flavour-tagging calibration to $B_s^0 \rightarrow D_s^\mp K^\pm$ decays, studied in simulation. This alternative decay-time fit is compared to the baseline fit and the difference in the results

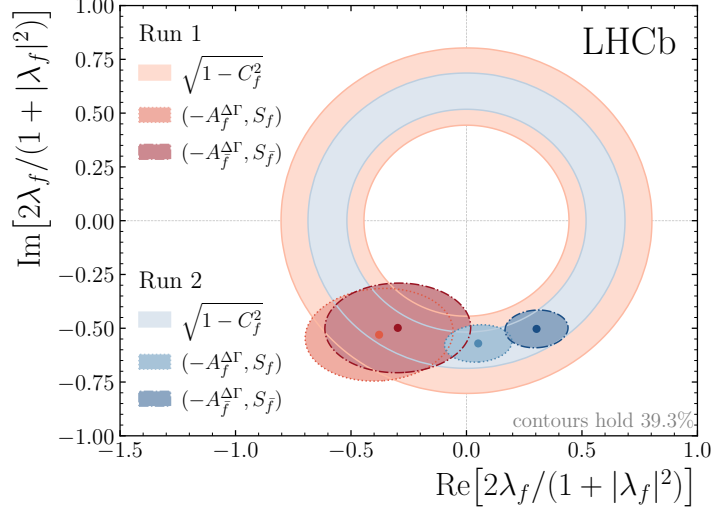


Figure 4: Representation of the CP observables in the $(\text{Re}[2\lambda_f/(1+|\lambda_f|^2)], \text{Im}[2\lambda_f/(1+|\lambda_f|^2)])$ Cartesian plane. The contours shown correspond to 39.3% of the distribution.

is assigned as a systematic uncertainty.

The remaining sources of systematic uncertainty are evaluated using pseudoexperiments, where each sample is generated according to the baseline results of the invariant-mass fit and, for the signal component, of the decay-time fit. The decay-time distributions of the backgrounds are generated to resemble the properties observed in data or found in simulation. The pseudoexperiments are processed using the same fit procedure as the data. To assess the systematic uncertainty, the parameter in question, considered for the systematic effect, is varied within its uncertainty. The values obtained from the baseline fit are compared to the values from the fits with the modified model. A distribution of the resulting differences is formed, taking into account the correlations between the baseline and modified pseudoexperiments. The systematic uncertainty is assigned as the mean and width of this distribution added in quadrature.

The systematic uncertainty related to the uncertainty on Δm_s , which is fixed in the baseline fit, is evaluated in a fit to pseudoexperiments in which the Δm_s value is shifted by one standard deviation. The difference between the result of the modified fit and baseline value is assigned as the systematic uncertainty. In a similar way, the systematic uncertainty related to the uncertainty on the uncorrelated parameter A_{det} is determined.

The systematic uncertainty from the limited knowledge of the decay-time resolution is obtained by repeating the fit to pseudoexperiments using a narrower or wider decay-time resolution model. The largest deviation between the baseline and modified fits is taken as the systematic uncertainty.

The correlation among the parameters Γ_s , $\Delta\Gamma_s$ and the decay-time acceptance obtained from the $B_s^0 \rightarrow D_s^- \pi^+$ data necessitates a combined treatment of the corresponding systematic uncertainties. The pseudoexperiments are fitted with modified values of the spline coefficients, as well as the Γ_s and $\Delta\Gamma_s$ parameters, which are sampled from the corresponding multidimensional correlated Gaussian distributions centred on their baseline values. The combined correlated systematic uncertainty is determined from the average deviation of these modified fits with respect to the baseline fits.

Table 3: Systematic uncertainties on the CP observables, expressed as a fraction of the corresponding statistical uncertainties. The value “—” indicates that the contribution is negligible.

Source	C_f	$A_f^{\Delta\Gamma}$	$A_{\bar{f}}^{\Delta\Gamma}$	S_f	$S_{\bar{f}}$
Invariant-mass fit	0.045	0.095	0.121	0.088	0.112
Flavour tagging	0.256	0.026	0.028	0.012	0.070
Oscillation frequency Δm_s	0.006	0.005	0.004	0.108	0.101
Detection asymmetry A_{det}	0.001	0.079	0.082	0.007	0.007
Decay-time resolution model	0.195	0.008	0.008	0.054	0.166
Decay-time acceptance, Γ_s , $\Delta\Gamma_s$	0.006	0.397	0.400	0.009	0.009
Decay-time acceptance simulation	0.004	0.064	0.064	—	0.004
Decay-time bias	0.062	0.027	0.046	0.188	0.167
Neglecting correlations	0.137	0.081	0.054	0.135	0.043
Total	0.358	0.430	0.439	0.277	0.293

As the decay-time acceptance obtained from the $B_s^0 \rightarrow D_s^- \pi^+$ data is corrected by the simulation, an additional source of systematic uncertainty arises from the limited size of the simulation samples that are used to determine the correction. To account for this, pseudoexperiments are fitted with a modified decay-time acceptance correction, that is sampled from a multidimensional Gaussian representing the uncertainties and correlations of the corrections. The average deviation of these modified fits with respect to the baseline fits is taken as a systematic uncertainty.

A decay-time bias is observed in the Δm_s measurement from the $B_s^0 \rightarrow D_s^- \pi^+$ decays [38], and corrected for in the baseline fit. A systematic uncertainty related to the uncertainty on the bias, taken to be ± 1 fs, is obtained using pseudoexperiments. This value includes both the uncertainty of the decay-time bias as obtained in the $B_s^0 \rightarrow D_s^- \pi^+$ decays and the correction to account for the differences in selection criteria between the two analyses [38].

The impact of neglecting the correlations among decay time and decay-time uncertainty with the B_s^0 and D_s^- invariant masses in the $sPlot$ method is studied with a dedicated set of pseudoexperiments using a bootstrapping method [52]. The method preserves correlations among observables. The results of the decay-time fits performed on samples with and without these correlations are compared and the mean difference is assigned as the systematic uncertainty.

Additional cross-checks are performed to further validate the results. The data sample is split into subsets according to the two LHCb dipole magnet polarity orientations, the year of data taking and the B_s^0 meson momentum. In addition, the data sample is split into decay-time bins and the invariant-mass fit is performed on each subsample. This is followed by the combined decay-time fit. In all cases, no significant deviations among the results are observed. A closure test using a large sample of simulated signal candidates provides an estimate of the intrinsic bias related to the decay-time fit procedure. No significant bias is found.

Several other potential systematic effects are examined but are found to be negligible. No significant systematic effect associated with the production asymmetry A_{prod} is observed. The decay-time fit is repeated by varying the knot positions in the decay-time acceptance

Table 4: Correlation matrix of the total systematic uncertainties of the CP observables.

Parameter	C_f	$A_f^{\Delta\Gamma}$	$A_{\bar{f}}^{\Delta\Gamma}$	S_f	$S_{\bar{f}}$
C_f	1	0.008	0.012	-0.080	-0.246
$A_f^{\Delta\Gamma}$		1	0.878	0.004	-0.022
$A_{\bar{f}}^{\Delta\Gamma}$			1	-0.002	-0.022
S_f				1	0.085
$S_{\bar{f}}$					1

description. No significant changes with respect to the baseline result are found. The precision on the world-average value for the oscillation frequency Δm_s is dominated by the LHCb measurement [38], which uses the same $B_s^0 \rightarrow D_s^- \pi^+$ sample used as a control channel in this analysis. The imperfect knowledge of the particles' momentum and the longitudinal dimension of the detector are encompassed by the systematic uncertainty on Δm_s , therefore these sources are not further considered.

The resulting systematic uncertainties are listed in Table 3 and expressed as fraction of the corresponding statistical uncertainties. The total systematic correlation matrix, reported in Table 4, is obtained by adding the covariance matrices corresponding to each source.

7 Interpretation

The measured CP -violating parameters listed in Table 1 can be interpreted in terms of the CKM angle γ , the strong phase difference δ , the magnitude of the amplitude ratio $r_{D_s K}$ and the mixing phase β_s . This is achieved using a frequentist approach detailed in Refs. [53, 54]. First, a likelihood function is defined as

$$\mathcal{L}(\vec{\alpha}) = \prod_i f(\vec{A}_i^{\text{obs}}|\vec{\alpha}), \quad (9)$$

where the function $f(\vec{A}_i^{\text{obs}}|\vec{\alpha})$ is assumed to follow a multivariate Gaussian distribution

$$f(\vec{A}_i^{\text{obs}}|\vec{\alpha}) \propto \exp\left(-\frac{1}{2}(\vec{A}(\vec{\alpha}) - \vec{A}_i^{\text{obs}})^T V_i^{-1} (\vec{A}(\vec{\alpha}) - \vec{A}_i^{\text{obs}})\right), \quad (10)$$

where \vec{A}_i^{obs} is the vector of observables ($C_f, A_f^{\Delta\Gamma}, A_{\bar{f}}^{\Delta\Gamma}, S_f, S_{\bar{f}}$), V_i is the experimental covariance matrix, and i is an index labelling the different measurements to be combined. The vector function $\vec{A}(\vec{\alpha})$ encodes the dependency of the observables on the parameters of interest $\vec{\alpha} = (\gamma, \beta_s, \delta, r_{D_s K})$, following Eq. 5. A fit is performed to find the set of values $\vec{\alpha}_{\text{min}}$ that minimise the function $\chi^2(\vec{\alpha}) = -2 \ln \mathcal{L}(\vec{\alpha})$. An ensemble of pseudoexperiments is generated to determine the best-fit values and confidence intervals of the parameters $\vec{\alpha}$, as detailed in Ref. [55]. This method is referred to as the *Plugin* method and is used throughout this paper for the results of γ , δ and $r_{D_s K}$.

As discussed in Sec. 1, the CP observables determined from $B_s^0 \rightarrow D_s^\mp K^\pm$ decays are functions of the weak-phase difference $(\gamma - 2\beta_s)$. Therefore, in order to determine γ , the value of β_s has to be taken from independent measurements. The value of β_s

Table 5: Updated values of the CP observables from the decay-time fit of the Run 1 analysis with updated values of the nuisance parameters Δm_s , Γ_s and $\Delta\Gamma_s$. The first uncertainty is statistical and the second is systematic.

Parameter	Value
C_f	$0.75 \pm 0.14 \pm 0.04$
$A_f^{\Delta\Gamma}$	$0.38 \pm 0.28 \pm 0.15$
$A_{\bar{f}}^{\Delta\Gamma}$	$0.30 \pm 0.28 \pm 0.15$
S_f	$-0.53 \pm 0.21 \pm 0.06$
$S_{\bar{f}}$	$-0.45 \pm 0.20 \pm 0.06$

is obtained through the relation $\phi_s = -2\beta_s$. Neglecting the contributions from loop diagrams, whose impact is estimated to be below the statistical uncertainty on ϕ_s [56], the value $\phi_s = -0.031 \pm 0.018$ rad is used, which is taken from the combination of LHCb measurements presented in Ref. [47].

The CP -violating parameters obtained from the Run 2 $B_s^0 \rightarrow D_s^\mp K^\pm$ data correspond to the following parameters:

$$\begin{aligned}\gamma &= (74 \pm 12)^\circ, \\ \delta &= (346.9_{-6.6}^{+6.8})^\circ, \\ r_{D_s K} &= 0.327_{-0.037}^{+0.039},\end{aligned}$$

where the phases γ and δ are determined up to a global shift of 180° , where the statistical and systematic uncertainties are summed in quadrature. Figure 5 shows the confidence-level (CL) plot for γ , as well as the two-dimensional contours of γ versus $r_{D_s K}$ and δ .

8 Combination with the results of the Run 1 analysis

The results of this measurement are combined with those obtained using Run 1 data, presented in Ref. [1]. To achieve that, the main systematic uncertainties of the Run 1 measurement related to the external parameters Γ_s , $\Delta\Gamma_s$ and Δm_s are recomputed using the more precise values considered in this analysis. These external parameters only affect the time-dependent part of the analysis, which is therefore updated with the new values. The following steps are repeated: the determination of the decay-time acceptance from $B_s^0 \rightarrow D_s^- \pi^+$ data, the flavour-tagging calibration, which is required because of its correlation with the Δm_s parameter in the fit to $B_s^0 \rightarrow D_s^- \pi^+$ data and the decay-time fit to $B_s^0 \rightarrow D_s^\mp K^\pm$ candidates to extract the values of the CP observables. Other aspects of the analysis, such as the decay-time resolution, obtained from calibration data, are unchanged with respect to Ref. [1]. The updated values of the CP observables from the Run 1 data set are reported in Table 5. Following the same procedure as described in Sec. 7, the values of the parameters γ , δ and $r_{D_s K}$ corresponding to the Run 1 measurement

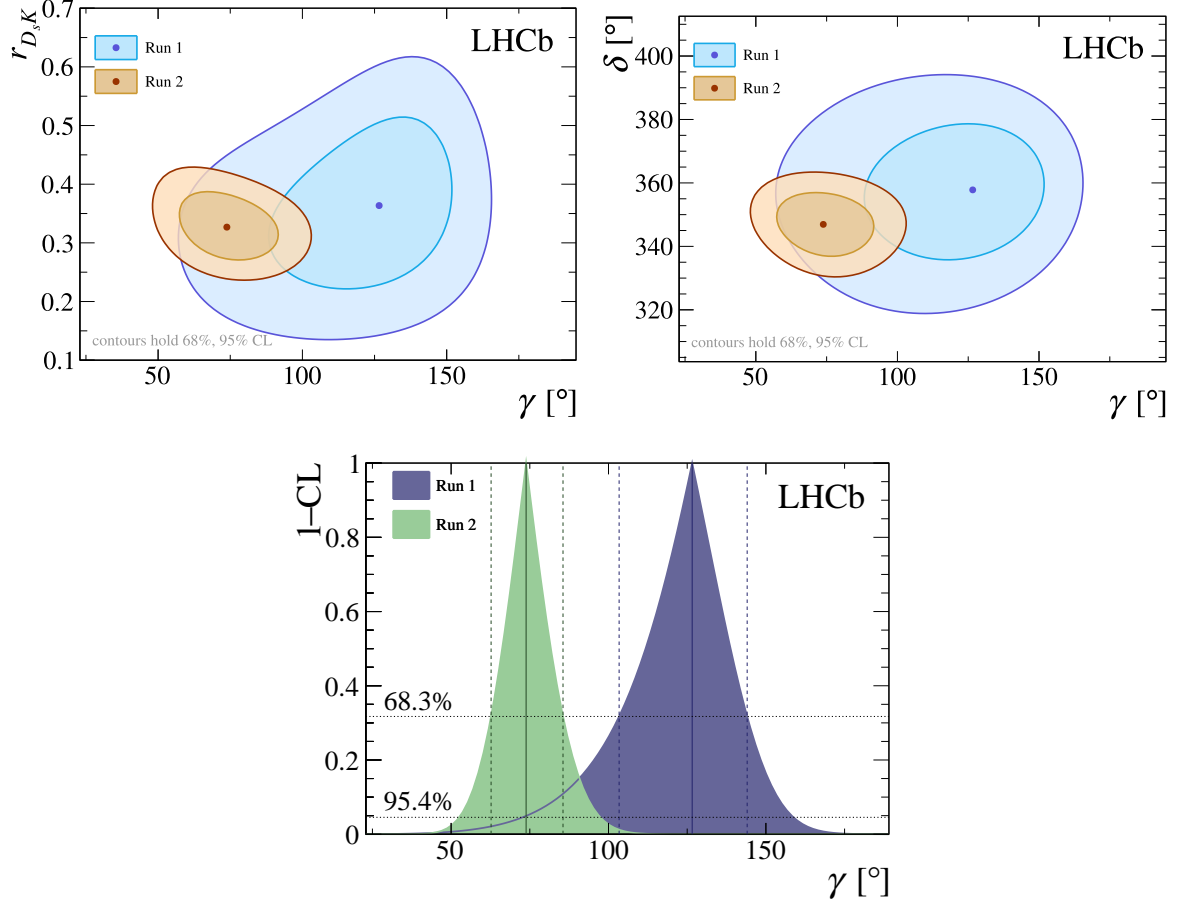


Figure 5: Contour plots of (top left) $r_{D_s K}$ vs. γ and (top right) δ vs. γ , where the contours correspond to the confidence levels (CL) of 68% and 95%. The bottom plot shows the $1 - CL$ curve for the angle γ , with the 68.3% and 95.4% CL intervals indicated with horizontal and vertical lines. The results correspond to $\gamma = (74 \pm 12)^\circ$ and $\gamma = (127^{+18}_{-26})^\circ$ for the Run 2 and Run 1 analysis, respectively, where updated values of Γ_s , $\Delta\Gamma_s$ and Δm_s are also propagated to the latter.

are

$$\begin{aligned}\gamma &= (127^{+18}_{-26})^\circ, \\ \delta &= (358^{+14}_{-15})^\circ, \\ r_{D_s K} &= 0.364^{+0.095}_{-0.094}.\end{aligned}$$

The Run 2 and the updated Run 1 results are compared in Fig. 5. The compatibility of γ , δ and $r_{D_s K}$ parameters between the updated Run 1 and the Run 2 results corresponds to a p -value of 12%.

The CP -violating parameters of the two data sets have been combined following the methods presented in Ref. [12]. The two measurements are treated as independent and the optimal values of γ , δ and $r_{D_s K}$ are obtained via the likelihood fit described in Sec. 7.

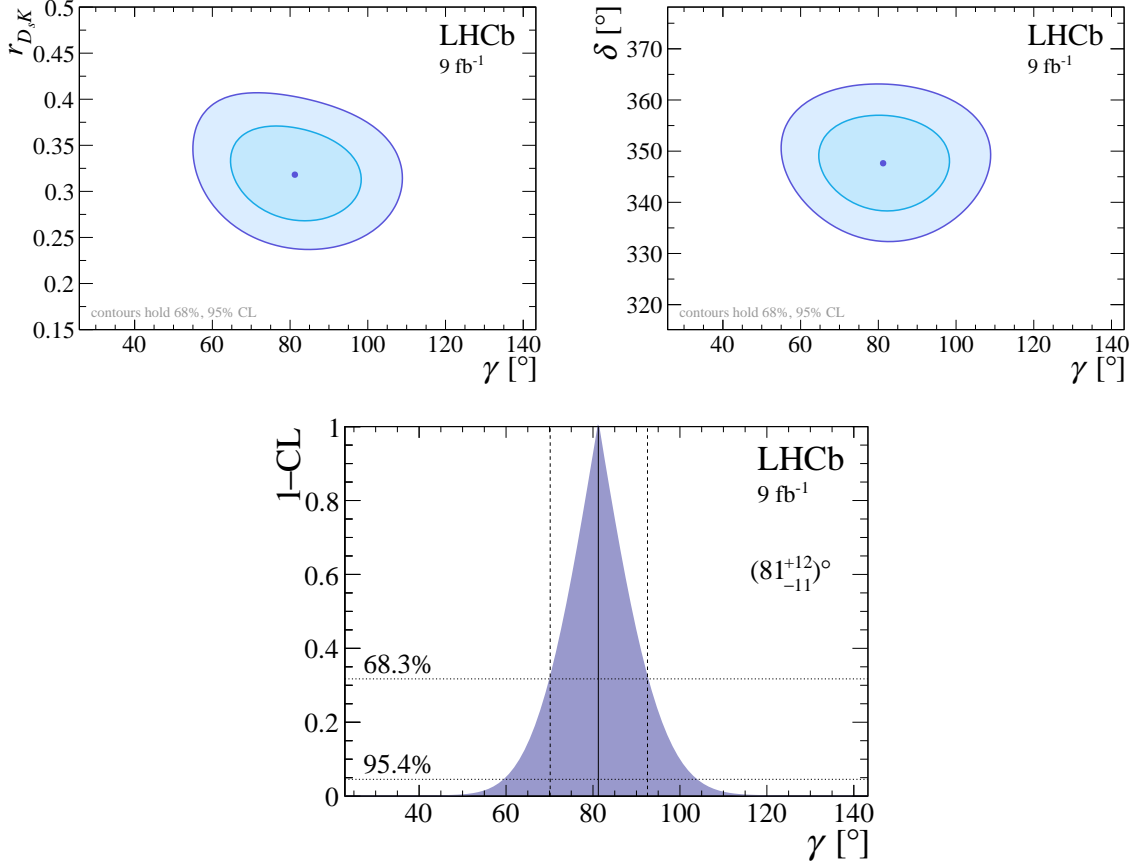


Figure 6: Contour plots arising from the combined extraction of γ , δ and $r_{D_s K}$ from the CP parameters from the Run 1 and Run 2 data sets. (Top left) $r_{D_s K}$ vs. γ and (top right) δ vs. γ , the contours correspond to the confidence levels (CL) of 68% and 95%. The bottom plot shows the $1 - \text{CL}$ curve for the angle γ , with the 68.3% and 95.4% CL intervals indicated with horizontal and vertical lines.

The resulting values are

$$\begin{aligned}\gamma &= (81^{+12}_{-11})^\circ, \\ \delta &= (347.6 \pm 6.3)^\circ, \\ r_{D_s K} &= 0.318^{+0.034}_{-0.033}.\end{aligned}$$

The corresponding $1 - \text{CL}$ curve for γ is shown in Fig. 6, as well as the two-dimensional contours of γ versus $r_{D_s K}$ and δ . Finally, the value of the relative weak-phase difference in $B_s^0 \rightarrow D_s^\mp K^\pm$ decays is determined to be $\gamma - 2\beta_s = (79^{+12}_{-11})^\circ$, providing complementary sensitivity to ϕ_s on a potential new physics phase in $B_s^0 - \bar{B}_s^0$ mixing.

9 Conclusion

The CP -violating parameters that describe the $B_s^0 \rightarrow D_s^\mp K^\pm$ decay rates have been measured using a data set corresponding to an integrated luminosity of 6 fb^{-1} of pp

collisions recorded with the LHCb detector. Their values are found to be

$$\begin{aligned}
C_f &= 0.791 \pm 0.061 \pm 0.022 , \\
A_f^{\Delta\Gamma} &= -0.051 \pm 0.134 \pm 0.058 , \\
A_{\bar{f}}^{\Delta\Gamma} &= -0.303 \pm 0.125 \pm 0.055 , \\
S_f &= -0.571 \pm 0.084 \pm 0.023 , \\
S_{\bar{f}} &= -0.503 \pm 0.084 \pm 0.025 ,
\end{aligned}$$

where the first uncertainties are statistical and the second are systematic. CP violation in the interference between $B_s^0-\bar{B}_s^0$ mixing and $B_s^0 \rightarrow D_s^\pm K^\pm$ decays is observed with a significance of 8.6σ . The results are used to determine the CKM angle γ , the strong-phase difference δ and the magnitude of the ratio $r_{D_s K}$ between the $B_s^0 \rightarrow D_s^+ K^-$ and the $B_s^0 \rightarrow D_s^- K^+$ decay amplitudes, leading to

$$\begin{aligned}
\gamma &= (74 \pm 12)^\circ , \\
\delta &= (346.9_{-6.6}^{+6.8})^\circ , \\
r_{D_s K} &= 0.327_{-0.037}^{+0.039} ,
\end{aligned}$$

where all angles are given modulo 180° , and uncertainties shown are the combination of the statistical and systematic contributions.

The results of the present analysis are combined with those from the previous LHCb analysis [1], which is updated to account for improved determinations of Γ_s , $\Delta\Gamma_s$ and Δm_s values. The following values of γ , δ and $r_{D_s K}$ are found from the combination:

$$\begin{aligned}
\gamma &= (81_{-11}^{+12})^\circ , \\
\delta &= (347.6 \pm 6.3)^\circ , \\
r_{D_s K} &= 0.318_{-0.033}^{+0.034} .
\end{aligned}$$

This value of γ represents the most precise determination of γ in B_s^0 meson decays and is in good agreement with the most recent LHCb γ combination [12].

Acknowledgements

We express our gratitude to our colleagues in the CERN accelerator departments for the excellent performance of the LHC. We thank the technical and administrative staff at the LHCb institutes. We acknowledge support from CERN and from the national agencies: CAPES, CNPq, FAPERJ and FINEP (Brazil); MOST and NSFC (China); CNRS/IN2P3 (France); BMBF, DFG and MPG (Germany); INFN (Italy); NWO (Netherlands); MNiSW and NCN (Poland); MCID/IFA (Romania); MICIU and AEI (Spain); SNSF and SER (Switzerland); NASU (Ukraine); STFC (United Kingdom); DOE NP and NSF (USA). We acknowledge the computing resources that are provided by CERN, IN2P3 (France), KIT and DESY (Germany), INFN (Italy), SURF (Netherlands), PIC (Spain), GridPP (United Kingdom), CSCS (Switzerland), IFIN-HH (Romania), CBPF (Brazil), and Polish WLCG (Poland). We are indebted to the communities behind the multiple open-source software packages on which we depend. Individual groups or members have received support from ARC and ARDC (Australia); Key Research Program of Frontier Sciences of CAS, CAS

PIFI, CAS CCEPP, Fundamental Research Funds for the Central Universities, and Sci. & Tech. Program of Guangzhou (China); Minciencias (Colombia); EPLANET, Marie Skłodowska-Curie Actions, ERC and NextGenerationEU (European Union); A*MIDEX, ANR, IPhU and Labex P2IO, and Région Auvergne-Rhône-Alpes (France); AvH Foundation (Germany); ICSC (Italy); Severo Ochoa and María de Maeztu Units of Excellence, GVA, XuntaGal, GENCAT, InTalent-Inditex and Prog. Atracción Talento CM (Spain); SRC (Sweden); the Leverhulme Trust, the Royal Society and UKRI (United Kingdom).

Appendices

A Dependence of the CP -violating parameters on external parameters for Run 2 data

The CP -violating parameters depend on external parameters such as the mixing frequency, Δm_s , the B_s^0 decay width, Γ_s , and the decay-width difference, $\Delta\Gamma_s$, which are fixed in the baseline $B_s^0 \rightarrow D_s^\mp K^\pm$ decay-time fit. The central values of these parameters might evolve over years, thus for any future combinations of the CKM angle γ it is important to evaluate the shift of the CP -violating parameters as a function of external parameters. This dependence on external parameters is calculated separately for Run 1 and Run 2 data-taking periods.

The dependence of the CP -violating parameters $A_f^{\Delta\Gamma}$ and $A_{\bar{f}}^{\Delta\Gamma}$ on $\Delta\Gamma_s$ is shown in Fig. 7 in the interval $\Delta\Gamma_s \in [0.075, 0.095]$ ps⁻¹. The horizontally and vertically hatched bands represent the statistical uncertainty of the $A_f^{\Delta\Gamma}$ and $A_{\bar{f}}^{\Delta\Gamma}$ parameters, while circles (squares) denote the difference of the $A_f^{\Delta\Gamma}$ ($A_{\bar{f}}^{\Delta\Gamma}$) parameter with respect to the baseline result. The interval is extended with respect to the baseline range, $\Delta\Gamma_s \in [0.081, 0.089]$ ps⁻¹, to account for the differences in the $\Delta\Gamma_s$ determination obtained with and without constraints from effective lifetime measurements [57]. The decay-time fit is repeated for ten alternative $\Delta\Gamma_s$ values within the extended interval. For these alternative fits the decay width, Γ_s , is fixed to be $\Gamma_s = 0.6563$ ps⁻¹. The difference of the CP -violating parameters with respect to the baseline result is evaluated. A small dependence is observed for the $A_f^{\Delta\Gamma}$ and $A_{\bar{f}}^{\Delta\Gamma}$ parameters. The first derivatives of the $A_f^{\Delta\Gamma}$ and $A_{\bar{f}}^{\Delta\Gamma}$ parameters with respect to the $\Delta\Gamma_s$ variable are determined to be 0.400 ± 0.012 ps and 3.13 ± 0.07 ps, respectively, for Run 2. For Run 1, the corresponding values are -4.26 ± 0.10 ps and -3.34 ± 0.08 ps. The derivatives are found to be negligible for the C_f , S_f and $S_{\bar{f}}$ parameters. Similarly, the dependence on the Γ_s parameter is studied and found to be negligible for all CP -violating observables.

The dependence of the CP -violating parameters on the mixing frequency, Δm_s , is obtained from pseudoexperiments, where the Δm_s value is shifted by one standard deviation with respect to the baseline value. In these alternative fits, the $\Delta\Gamma_s$ parameter is fixed to be $\Delta\Gamma_s = 0.085$ ps⁻¹. The first derivatives of S_f and $S_{\bar{f}}$ computed with respect to the Δm_s variable are evaluated to be 1.712 ± 0.011 ps and -1.653 ± 0.011 ps, respectively, for Run 2. For Run 1, the corresponding values are 1.6 ± 0.9 ps and -1.5 ± 1.0 ps. The dependencies are found to be negligible for the C_f , $A_f^{\Delta\Gamma}$ and $A_{\bar{f}}^{\Delta\Gamma}$ parameters.

B Total statistical and systematic correlation matrices for the updated Run 1 result

For the combination of Run 1 and Run 2 results described in Sec. 8 the decay-time fit of the Run 1 measurement is updated with more recent values of input parameters used in the present analysis of Run 2 data. For reference, the correlation matrix of the five parameters extracted in the updated fit is given in Table 6. Additionally, the update implies the need to reevaluate some of the systematic uncertainties. The systematic uncertainties in the Run 1 measurement introduced by the limited knowledge of the

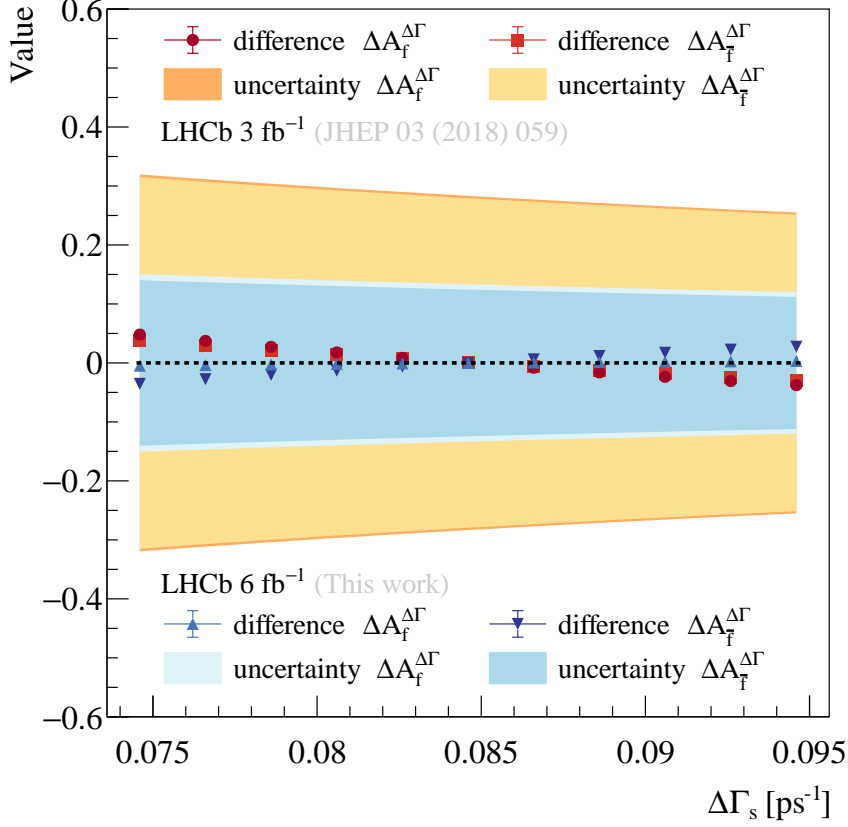


Figure 7: Dependence of the CP -violating parameters $A_f^{\Delta\Gamma}$ and $A_{\bar{f}}^{\Delta\Gamma}$ on the $\Delta\Gamma_s$ parameter. The triangles, circles and squares denote the differences in the $A_f^{\Delta\Gamma}$ and $A_{\bar{f}}^{\Delta\Gamma}$ parameters with respect to the baseline result. For comparison, the orange and blue bands visualise the size of the statistical uncertainty of the $A_f^{\Delta\Gamma}$ and $A_{\bar{f}}^{\Delta\Gamma}$ parameters as obtained in the corresponding fits to Run 1 and Run 2 data, respectively.

Table 6: Statistical correlation matrix of the CP observables in the updated fit of the Run 1 data set.

Parameter	C_f	$A_f^{\Delta\Gamma}$	$A_{\bar{f}}^{\Delta\Gamma}$	S_f	$S_{\bar{f}}$
C_f	1	0.114	0.098	0.018	-0.054
$A_f^{\Delta\Gamma}$		1	0.546	-0.088	-0.024
$A_{\bar{f}}^{\Delta\Gamma}$			1	-0.051	-0.024
S_f				1	0.001
$S_{\bar{f}}$					1

parameters Δm_s , Γ_s , $\Delta\Gamma_s$ and the decay-time acceptance model are evaluated with the same pseudoexperiment-based approach as described in Sec. 6. The total systematic uncertainty, with updated contributions, is reported together with the updated statistical uncertainty in Table 5. For completeness, the correlation matrix of the combined and partially updated systematic uncertainty of the Run 1 measurement is provided in Table 7.

Table 7: Systematic correlation matrix of the CP observables in the updated fit of the Run 1 data set.

Parameter	C_f	$A_f^{\Delta\Gamma}$	$A_{\bar{f}}^{\Delta\Gamma}$	S_f	$S_{\bar{f}}$
C_f	1	0.07	0.05	0.04	-0.01
$A_f^{\Delta\Gamma}$		1	0.53	0.02	0.02
$A_{\bar{f}}^{\Delta\Gamma}$			1	0.03	0.03
S_f				1	0.02
$S_{\bar{f}}$					1

References

- [1] LHCb collaboration, R. Aaij *et al.*, *Measurement of CP asymmetry in $B_s^0 \rightarrow D_s^\mp K^\pm$ decays*, JHEP **03** (2018) 059, [arXiv:1712.07428](#).
- [2] LHCb collaboration, R. Aaij *et al.*, *Measurement of CP violation in $B^0 \rightarrow D^\pm \pi^\mp$ decays*, JHEP **06** (2018) 084, [arXiv:1805.03448](#).
- [3] BaBar collaboration, B. Aubert *et al.*, *Measurement of time-dependent CP-violating asymmetries and constraints on $\sin(2\beta + \gamma)$ with partial reconstruction of $B \rightarrow D^{*\mp} \pi^\pm$ decays*, Phys. Rev. **D71** (2005) 112003, [arXiv:hep-ex/0504035](#).
- [4] BaBar collaboration, B. Aubert *et al.*, *Measurement of time-dependent CP asymmetries in $B^0 \rightarrow D^{(*)\pm} \pi^\mp$ and $B^0 \rightarrow D^\pm \rho^\mp$* , Phys. Rev. **D73** (2006) 111101(R), [arXiv:hep-ex/0602049](#).
- [5] Belle collaboration, F. J. Ronga *et al.*, *Measurements of CP violation in $B^0 \rightarrow D^{*-} \pi^+$ and $B^0 \rightarrow D^- \pi^+$ decays*, Phys. Rev. **D73** (2006) 092003, [arXiv:hep-ex/0604013](#).
- [6] Belle collaboration, S. Bahinipati *et al.*, *Measurements of time-dependent CP asymmetries in $B \rightarrow D^{*\mp} \pi^\pm$ decays using a partial reconstruction technique*, Phys. Rev. **D84** (2011) 021101, [arXiv:1102.0888](#).
- [7] N. Cabibbo, *Unitary symmetry and leptonic decays*, Phys. Rev. Lett. **10** (1963) 531.
- [8] M. Kobayashi and T. Maskawa, *CP violation in the renormalizable theory of weak interaction*, Prog. Theor. Phys. **49** (1973) 652.
- [9] C. Jarlskog, *Commutator of the quark mass matrices in the standard electroweak model and a measure of maximal CP nonconservation*, Phys. Rev. Lett. **55** (1985) 1039.
- [10] C. Jarlskog, *Jarlskog responds*, Phys. Rev. Lett. **57** (1986) 2875.
- [11] R. Huerta and R. Pérez-Marcial, *Comment on “Commutator of the quark mass matrices in the standard electroweak model and a measure of maximal CP nonconservation”*, Phys. Rev. Lett. **58** (1987) 1698.

- [12] LHCb collaboration, *Simultaneous determination of the CKM angle γ and parameters related to mixing and CP violation in the charm sector*, LHCb-CONF-2024-004, 2024; LHCb collaboration, R. Aaij *et al.*, *Simultaneous determination of CKM angle γ and charm mixing parameters*, JHEP **12** (2021) 141, arXiv:2110.02350.
- [13] I. Dunietz and R. G. Sachs, *Asymmetry between inclusive charmed and anticharmed modes in B^0 , \bar{B}^0 decay as a measure of CP violation*, Phys. Rev. **D37** (1988) 3186, Erratum *ibid.* **D39** (1989) 3515.
- [14] R. Aleksan, I. Dunietz, and B. Kayser, *Determining the CP violating phase γ* , Z. Phys. **C54** (1992) 653.
- [15] R. Fleischer, *New strategies to obtain insights into CP violation through $B_{(s)} \rightarrow D_{(s)}^\pm K^\mp, D_{(s)}^{*\pm} K^\mp, \dots$ and $B_{(d)} \rightarrow D^\pm \pi^\mp, D^{*\pm} \pi^\mp, \dots$ decays*, Nucl. Phys. **B671** (2003) 459, arXiv:hep-ph/0304027.
- [16] K. De Bruyn *et al.*, *Exploring $B_s \rightarrow D_s^{(*)\pm} K^\mp$ decays in the presence of a sizable width difference $\Delta\Gamma_s$* , Nucl. Phys. **B868** (2013) 351, arXiv:1208.6463.
- [17] R. Fleischer and E. Malami, *Revealing new physics in $B_s^0 \rightarrow D_s^\mp K^\pm$ decays*, Eur. Phys. J. C **83** (2023) 420, arXiv:2110.04240.
- [18] R. Fleischer and E. Malami, *Using $B_s^0 \rightarrow D_s^\mp K^\pm$ Decays as a Portal to New Physics*, Phys. Rev. D **106** (2022) 056004, arXiv:2109.04950.
- [19] LHCb collaboration, R. Aaij *et al.*, *Measurement of the branching fraction of the $B^0 \rightarrow D_s^+ \pi^-$ decay*, Eur. Phys. J. **C81** (2021) 314, arXiv:2010.11986.
- [20] L. Wolfenstein, *Parametrization of the Kobayashi-Maskawa matrix*, Phys. Rev. Lett. **51** (1983) 1945.
- [21] Particle Data Group, N. S. *et al.*, *Review of particle physics*, to be published in Phys. Rev **D110** (2024) 030001.
- [22] R. Aaij *et al.*, *Design and performance of the LHCb trigger and full real-time reconstruction in Run 2 of the LHC*, JINST **14** (2019) P04013, arXiv:1812.10790.
- [23] M. Pivk and F. R. Le Diberder, *sPlot: A statistical tool to unfold data distributions*, Nucl. Instrum. Meth. **A555** (2005) 356, arXiv:physics/0402083.
- [24] LHCb collaboration, R. Aaij *et al.*, *Measurement of the CP asymmetry in $B_s^0 - \bar{B}_s^0$ mixing*, Phys. Rev. Lett. **117** (2016) 061803, arXiv:1605.09768.
- [25] LHCb collaboration, A. A. Alves Jr. *et al.*, *The LHCb detector at the LHC*, JINST **3** (2008) S08005.
- [26] LHCb collaboration, R. Aaij *et al.*, *LHCb detector performance*, Int. J. Mod. Phys. **A30** (2015) 1530022, arXiv:1412.6352.
- [27] V. V. Gligorov and M. Williams, *Efficient, reliable and fast high-level triggering using a bonsai boosted decision tree*, JINST **8** (2013) P02013, arXiv:1210.6861.

- [28] T. Likhomanenko *et al.*, *LHCb topological trigger reoptimization*, J. Phys. Conf. Ser. **664** (2015) 082025, [arXiv:1510.00572](#).
- [29] T. Sjöstrand, S. Mrenna, and P. Skands, *A brief introduction to PYTHIA 8.1*, Comput. Phys. Commun. **178** (2008) 852, [arXiv:0710.3820](#); T. Sjöstrand, S. Mrenna, and P. Skands, *PYTHIA 6.4 physics and manual*, JHEP **05** (2006) 026, [arXiv:hep-ph/0603175](#).
- [30] I. Belyaev *et al.*, *Handling of the generation of primary events in Gauss, the LHCb simulation framework*, J. Phys. Conf. Ser. **331** (2011) 032047.
- [31] D. J. Lange, *The EvtGen particle decay simulation package*, Nucl. Instrum. Meth. **A462** (2001) 152.
- [32] N. Davidson, T. Przedzinski, and Z. Was, *PHOTOS interface in C++: Technical and physics documentation*, Comp. Phys. Comm. **199** (2016) 86, [arXiv:1011.0937](#).
- [33] Geant4 collaboration, J. Allison *et al.*, *Geant4 developments and applications*, IEEE Trans. Nucl. Sci. **53** (2006) 270; Geant4 collaboration, S. Agostinelli *et al.*, *Geant4: A simulation toolkit*, Nucl. Instrum. Meth. **A506** (2003) 250.
- [34] M. Clemencic *et al.*, *The LHCb simulation application, Gauss: Design, evolution and experience*, J. Phys. Conf. Ser. **331** (2011) 032023.
- [35] W. D. Hulsbergen, *Decay chain fitting with a Kalman filter*, Nucl. Instrum. Meth. **A552** (2005) 566, [arXiv:physics/0503191](#).
- [36] L. Breiman, J. H. Friedman, R. A. Olshen, and C. J. Stone, *Classification and regression trees*, Wadsworth international group, Belmont, California, USA, 1984.
- [37] B. P. Roe *et al.*, *Boosted decision trees as an alternative to artificial neural networks for particle identification*, Nucl. Instrum. Meth. **A543** (2005) 577, [arXiv:physics/0408124](#).
- [38] LHCb collaboration, R. Aaij *et al.*, *Precise determination of the B_s^0 - \bar{B}_s^0 oscillation frequency*, Nature Physics **18** (2022) 1, [arXiv:2104.04421](#).
- [39] K. Heinicke, *Measurement of the oscillation frequency Δm_s at LHCb*, PhD thesis, TU Dortmund, 2021, doi: <http://dx.doi.org/10.17877/DE290R-22378>.
- [40] R. Aaij *et al.*, *Selection and processing of calibration samples to measure the particle identification performance of the LHCb experiment in Run 2*, Eur. Phys. J. Tech. Instr. **6** (2019) 1, [arXiv:1803.00824](#).
- [41] D. Martínez Santos and F. Dupertuis, *Mass distributions marginalized over per-event errors*, Nucl. Instrum. Meth. **A764** (2014) 150, [arXiv:1312.5000](#).
- [42] N. L. Johnson, *Systems of frequency curves generated by methods of translation*, Biometrika **36** (1949) 149.
- [43] K. S. Cranmer, *Kernel estimation in high-energy physics*, Comput. Phys. Commun. **136** (2001) 198, [arXiv:hep-ex/0011057](#).

- [44] LHCb collaboration, R. Aaij *et al.*, *Opposite-side flavour tagging of B mesons at the LHCb experiment*, Eur. Phys. J. **C72** (2012) 2022, [arXiv:1202.4979](#).
- [45] LHCb collaboration, R. Aaij *et al.*, *B flavour tagging using charm decays at the LHCb experiment*, JINST **10** (2015) P10005, [arXiv:1507.07892](#).
- [46] LHCb collaboration, R. Aaij *et al.*, *A new algorithm for identifying the flavour of B_s^0 mesons at LHCb*, JINST **11** (2016) P05010, [arXiv:1602.07252](#).
- [47] LHCb collaboration, R. Aaij *et al.*, *Improved measurement of CP violation parameters in $B_s^0 \rightarrow J/\psi K^+ K^-$ decays in the vicinity of the $\phi(1020)$ resonance*, Phys. Rev. Lett. **132** (2024) 051802, [arXiv:2308.01468](#).
- [48] M. Karbach, G. Raven, and M. Schiller, *Decay time integrals in neutral meson mixing and their efficient evaluation*, [arXiv:1407.0748](#).
- [49] A. Davis *et al.*, *Measurement of the instrumental asymmetry for $K^- \pi^+$ -pairs at LHCb in Run 2*, LHCb-PUB-2018-004, 2018.
- [50] LHCb collaboration, R. Aaij *et al.*, *Measurement of CP observables in $B^\pm \rightarrow D^{(*)} K^\pm$ and $B^\pm \rightarrow D^{(*)} \pi^\pm$ decays using two-body D final states*, JHEP **04** (2021) 081, [arXiv:2012.09903](#).
- [51] C. Langenbruch, *Parameter uncertainties in weighted unbinned maximum likelihood fits*, Eur. Phys. J. **C82** (2022) 393, [arXiv:1911.01303](#).
- [52] B. Efron, *Bootstrap methods: Another look at the jackknife*, Ann. Statist. **7** (1979) 1.
- [53] M. Kenzie *et al.*, *GammaCombo: A statistical analysis framework for combining measurements, fitting datasets and producing confidence intervals*, doi: 10.5281/zenodo.3371421.
- [54] LHCb collaboration, R. Aaij *et al.*, *Measurement of the CKM angle γ from a combination of LHCb results*, JHEP **12** (2016) 087, [arXiv:1611.03076](#).
- [55] S. Bodhisattva, M. Walker, and M. Woodroffe, *On the Unified Method with nuisance Parameters*, Statist. Sinica **19** (2009) 301.
- [56] M. Z. Barel, K. De Bruyn, R. Fleischer, and E. Malami, *In pursuit of new physics with $B_d^0 \rightarrow J/\psi K^0$ and $B_s^0 \rightarrow J/\psi \phi$ decays at the high-precision Frontier*, J. Phys. G **48** (2021) 065002, [arXiv:2010.14423](#).
- [57] Y. Amhis *et al.*, *Averages of b-hadron, c-hadron, and τ -lepton properties as of 2021*, Phys. Rev. **D107** (2023) 052008, [arXiv:2206.07501](#), updated results and plots available at <https://hflav.web.cern.ch>.

LHCb collaboration

R. Aaij³⁶ , A.S.W. Abdelmotteleb⁵⁵ , C. Abellan Beteta⁴⁹ , F. Abudinén⁵⁵ ,
T. Ackernley⁵⁹ , A. A. Adefisoye⁶⁷ , B. Adeva⁴⁵ , M. Adinolfi⁵³ , P. Adlarson⁸⁰ ,
C. Agapopoulou¹³ , C.A. Aidala⁸¹ , Z. Ajaltouni¹¹ , S. Akar⁶⁴ , K. Akiba³⁶ ,
P. Albicocco²⁶ , J. Albrecht^{18,g} , F. Alessio⁴⁷ , M. Alexander⁵⁸ , Z. Aliouche⁶¹ ,
P. Alvarez Cartelle⁵⁴ , R. Amalric¹⁵ , S. Amato³ , J.L. Amey⁵³ , Y. Amhis^{13,47} ,
L. An⁶ , L. Anderlini²⁵ , M. Andersson⁴⁹ , A. Andreianov⁴² , P. Andreola⁴⁹ ,
M. Andreotti²⁴ , D. Andreou⁶⁷ , A. Anelli^{29,p} , D. Ao⁷ , F. Archilli^{35,v} ,
M. Argenton²⁴ , S. Arguedas Cuendis^{9,47} , A. Artamonov⁴² , M. Artuso⁶⁷ ,
E. Aslanides¹² , R. Ataíde Da Silva⁴⁸ , M. Atzeni⁶³ , B. Audurier¹⁴ , D. Bacher⁶² ,
I. Bachiller Perea¹⁰ , S. Bachmann²⁰ , M. Bachmayer⁴⁸ , J.J. Back⁵⁵ ,
P. Baladron Rodriguez⁴⁵ , V. Balagura¹⁴ , W. Baldini²⁴ , L. Balzani¹⁸ , H. Bao⁷ ,
J. Baptista de Souza Leite⁵⁹ , C. Barbero Pretel^{45,82} , M. Barbetti²⁵ , I. R. Barbosa⁶⁸ ,
R.J. Barlow⁶¹ , M. Barnyakov²³ , S. Barsuk¹³ , W. Barter⁵⁷ , M. Bartolini⁵⁴ ,
J. Bartz⁶⁷ , J.M. Basels¹⁶ , S. Bashir³⁸ , G. Bassi^{33,s} , B. Batsukh⁵ , P. B. Battista¹³ ,
A. Bay⁴⁸ , A. Beck⁵⁵ , M. Becker¹⁸ , F. Bedeschi³³ , I.B. Bediaga² , N. A.
Behling¹⁸ , S. Belin⁴⁵ , V. Bellee⁴⁹ , K. Belous⁴² , I. Belov²⁷ , I. Belyaev³⁴ ,
G. Benane¹² , G. Bencivenni²⁶ , E. Ben-Haim¹⁵ , A. Berezhnoy⁴² , R. Bernet⁴⁹ ,
S. Bernet Andres⁴³ , A. Bertolin³¹ , C. Betancourt⁴⁹ , F. Betti⁵⁷ , J. Bex⁵⁴ ,
Ia. Bezshyiko⁴⁹ , J. Bhom³⁹ , M.S. Bieker¹⁸ , N.V. Biesuz²⁴ , P. Billoir¹⁵ ,
A. Biolchini³⁶ , M. Birch⁶⁰ , F.C.R. Bishop¹⁰ , A. Bitadze⁶¹ , A. Bizzeti , T. Blake⁵⁵ ,
F. Blanc⁴⁸ , J.E. Blank¹⁸ , S. Blusk⁶⁷ , V. Bocharnikov⁴² , J.A. Boelhaue¹⁸ ,
O. Boente Garcia¹⁴ , T. Boettcher⁶⁴ , A. Bohare⁵⁷ , A. Boldyrev⁴² , C.S. Bolognani⁷⁷ ,
R. Bolzonella^{24,m} , N. Bondar⁴² , A. Bordelius⁴⁷ , F. Borgato^{31,q} , S. Borghi⁶¹ ,
M. Borsato^{29,p} , J.T. Borsuk³⁹ , S.A. Bouchiba⁴⁸ , M. Bovill⁶² , T.J.V. Bowcock⁵⁹ ,
A. Boyer⁴⁷ , C. Bozzi²⁴ , A. Brea Rodriguez⁴⁸ , N. Breer¹⁸ , J. Brodzicka³⁹ ,
A. Brossa Gonzalo^{45,55,44,†} , J. Brown⁵⁹ , D. Brundu³⁰ , E. Buchanan⁵⁷ , A. Buonauro⁴⁹ ,
L. Buonincontri^{31,q} , A.T. Burke⁶¹ , C. Burr⁴⁷ , J.S. Butter⁵⁴ , J. Buytaert⁴⁷ ,
W. Byczynski⁴⁷ , S. Cadeddu³⁰ , H. Cai⁷² , A. C. Caillet¹⁵ , R. Calabrese^{24,m} ,
S. Calderon Ramirez⁹ , L. Calefice⁴⁴ , S. Cali²⁶ , M. Calvi^{29,p} , M. Calvo Gomez⁴³ ,
P. Camargo Magalhaes^{2,z} , J. I. Cambon Bouzas⁴⁵ , P. Campana²⁶ ,
D.H. Campora Perez⁷⁷ , A.F. Campoverde Quezada⁷ , S. Capelli²⁹ , L. Capriotti²⁴ ,
R. Caravaca-Mora⁹ , A. Carbone^{23,k} , L. Carcedo Salgado⁴⁵ , R. Cardinale^{27,n} ,
A. Cardini³⁰ , P. Carniti^{29,p} , L. Carus²⁰ , A. Casais Vidal⁶³ , R. Caspary²⁰ ,
G. Casse⁵⁹ , J. Castro Godinez⁹ , M. Cattaneo⁴⁷ , G. Cavallero^{24,47} , V. Cavallini^{24,m} ,
S. Celani²⁰ , D. Cervenkov⁶² , S. Cesare^{28,o} , A.J. Chadwick⁵⁹ , I. Chahrour⁸¹ ,
M. Charles¹⁵ , Ph. Charpentier⁴⁷ , E. Chatzianagnostou³⁶ , M. Chefdeville¹⁰ ,
C. Chen¹² , S. Chen⁵ , Z. Chen⁷ , A. Chernov³⁹ , S. Chernyshenko⁵¹ , X.
Chiotopoulos⁷⁷ , V. Chobanova⁷⁹ , S. Cholak⁴⁸ , M. Chrzaszcz³⁹ , A. Chubykin⁴² ,
V. Chulikov⁴² , P. Ciambone²⁶ , X. Cid Vidal⁴⁵ , G. Ciezarek⁴⁷ , P. Cifra⁴⁷ ,
P.E.L. Clarke⁵⁷ , M. Clemencic⁴⁷ , H.V. Cliff⁵⁴ , J. Closier⁴⁷ , C. Cocha Toapaxi²⁰ ,
V. Coco⁴⁷ , J. Cogan¹² , E. Cogneras¹¹ , L. Cojocariu⁴¹ , P. Collins⁴⁷ ,
T. Colombo⁴⁷ , M. Colonna¹⁸ , A. Comerma-Montells⁴⁴ , L. Congedo²² , A. Contu³⁰ ,
N. Cooke⁵⁸ , I. Corredoira⁴⁵ , A. Correia¹⁵ , G. Corti⁴⁷ , J.J. Cottee Meldrum⁵³ ,
B. Couturier⁴⁷ , D.C. Craik⁴⁹ , M. Cruz Torres^{2,h} , E. Curras Rivera⁴⁸ , R. Currie⁵⁷ ,
C.L. Da Silva⁶⁶ , S. Dadabaev⁴² , L. Dai⁶⁹ , X. Dai⁶ , E. Dall'Occo¹⁸ , J. Dalseno⁴⁵ ,
C. D'Ambrosio⁴⁷ , J. Daniel¹¹ , A. Danilina⁴² , P. d'Argent²² , A. Davidson⁵⁵ ,
J.E. Davies⁶¹ , A. Davis⁶¹ , O. De Aguiar Francisco⁶¹ , C. De Angelis^{30,l} ,
F. De Benedetti⁴⁷ , J. de Boer³⁶ , K. De Bruyn⁷⁶ , S. De Capua⁶¹ , M. De Cian^{20,47} 

D.J. Unverzagt²⁰ , E. Ursov⁴² , A. Usachov³⁷ , A. Ustyuzhanin⁴² , U. Uwer²⁰ ,
V. Vagnoni²³ , V. Valcarce Cadenas⁴⁵ , G. Valenti²³ , N. Valls Canudas⁴⁷ ,
H. Van Hecke⁶⁶ , E. van Herwijnen⁶⁰ , C.B. Van Hulse^{45,y} , R. Van Laak⁴⁸ ,
M. van Veghel³⁶ , G. Vasquez⁴⁹ , R. Vazquez Gomez⁴⁴ , P. Vazquez Regueiro⁴⁵ ,
C. Vázquez Sierra⁴⁵ , S. Vecchi²⁴ , J.J. Velthuis⁵³ , M. Veltri^{25,x} , A. Venkateswaran⁴⁸ ,
M. Veronesi³⁶ , M. Vesterinen⁵⁵ , D. Vico Benet⁶² , P. Vidrier Villalba⁴⁴ ,
M. Vieites Diaz⁴⁷ , X. Vilasis-Cardona⁴³ , E. Vilella Figueras⁵⁹ , A. Villa²³ ,
P. Vincent¹⁵ , F.C. Volle⁵² , D. vom Bruch¹² , N. Voropaev⁴² , K. Vos⁷⁷ ,
G. Vouters^{10,47} , C. Vrahas⁵⁷ , J. Wagner¹⁸ , J. Walsh³³ , E.J. Walton^{1,55} , G. Wan⁶ ,
C. Wang²⁰ , G. Wang⁸ , H. Wang⁷¹ , J. Wang⁶ , J. Wang⁵ , J. Wang^{4,c} , J. Wang⁷² ,
M. Wang²⁸ , N. W. Wang⁷ , R. Wang⁵³ , X. Wang⁸ , X. Wang⁷⁰ , X. W. Wang⁶⁰ ,
Y. Wang⁶ , Y. W. Wang⁷¹ , Z. Wang¹³ , Z. Wang^{4,c} , Z. Wang²⁸ , J.A. Ward^{55,1} ,
M. Waterlaet⁴⁷ , N.K. Watson⁵² , D. Websdale⁶⁰ , Y. Wei⁶ , J. Wendel⁷⁹ ,
B.D.C. Westhenry⁵³ , C. White⁵⁴ , M. Whitehead⁵⁸ , E. Whiter⁵² ,
A.R. Wiederhold⁶¹ , D. Wiedner¹⁸ , G. Wilkinson⁶² , M.K. Wilkinson⁶⁴ ,
M. Williams⁶³ , M.R.J. Williams⁵⁷ , R. Williams⁵⁴ , Z. Williams⁵³ , F.F. Wilson⁵⁶ ,
W. Wislicki⁴⁰ , M. Witek³⁹ , L. Witola²⁰ , G. Wormser¹³ , S.A. Wotton⁵⁴ , H. Wu⁶⁷ ,
J. Wu⁸ , Y. Wu⁶ , Z. Wu⁷ , K. Wyllie⁴⁷ , S. Xian⁷⁰ , Z. Xiang⁵ , Y. Xie⁸ , A. Xu³³ ,
J. Xu⁷ , L. Xu^{4,c} , L. Xu^{4,c} , M. Xu⁵⁵ , Z. Xu⁴⁷ , Z. Xu⁷ , Z. Xu⁵ , D. Yang⁴ , K.
Yang⁶⁰ , S. Yang⁷ , X. Yang⁶ , Y. Yang^{27,n} , Z. Yang⁶ , Z. Yang⁶⁵ ,
V. Yeroshenko¹³ , H. Yeung⁶¹ , H. Yin⁸ , X. Yin⁷ , C. Y. Yu⁶ , J. Yu⁶⁹ ,
X. Yuan⁵ , Y. Yuan^{5,7} , E. Zaffaroni⁴⁸ , M. Zavertyaev¹⁹ , M. Zdybal³⁹ ,
F. Zenesini^{23,k} , C. Zeng^{5,7} , M. Zeng^{4,c} , C. Zhang⁶ , D. Zhang⁸ , J. Zhang⁷ ,
L. Zhang^{4,c} , S. Zhang⁶⁹ , S. Zhang⁶² , Y. Zhang⁶ , Y. Z. Zhang^{4,c} , Y. Zhao²⁰ ,
A. Zharkova⁴² , A. Zhelezov²⁰ , S. Z. Zheng⁶ , X. Z. Zheng^{4,c} , Y. Zheng⁷ ,
T. Zhou⁶ , X. Zhou⁸ , Y. Zhou⁷ , V. Zhovkovska⁵⁵ , L. Z. Zhu⁷ , X. Zhu^{4,c} ,
X. Zhu⁸ , V. Zhukov¹⁶ , J. Zhuo⁴⁶ , Q. Zou^{5,7} , D. Zuliani^{31,q} , G. Zunica⁴⁸ .

¹*School of Physics and Astronomy, Monash University, Melbourne, Australia*

²*Centro Brasileiro de Pesquisas Físicas (CBPF), Rio de Janeiro, Brazil*

³*Universidade Federal do Rio de Janeiro (UFRJ), Rio de Janeiro, Brazil*

⁴*Department of Engineering Physics, Tsinghua University, Beijing, China*

⁵*Institute Of High Energy Physics (IHEP), Beijing, China*

⁶*School of Physics State Key Laboratory of Nuclear Physics and Technology, Peking University, Beijing, China*

⁷*University of Chinese Academy of Sciences, Beijing, China*

⁸*Institute of Particle Physics, Central China Normal University, Wuhan, Hubei, China*

⁹*Consejo Nacional de Rectores (CONARE), San Jose, Costa Rica*

¹⁰*Université Savoie Mont Blanc, CNRS, IN2P3-LAPP, Annecy, France*

¹¹*Université Clermont Auvergne, CNRS/IN2P3, LPC, Clermont-Ferrand, France*

¹²*Aix Marseille Univ, CNRS/IN2P3, CPPM, Marseille, France*

¹³*Université Paris-Saclay, CNRS/IN2P3, IJCLab, Orsay, France*

¹⁴*Laboratoire Leprince-Ringuet, CNRS/IN2P3, Ecole Polytechnique, Institut Polytechnique de Paris, Palaiseau, France*

¹⁵*LPNHE, Sorbonne Université, Paris Diderot Sorbonne Paris Cité, CNRS/IN2P3, Paris, France*

¹⁶*I. Physikalisches Institut, RWTH Aachen University, Aachen, Germany*

¹⁷*Universität Bonn - Helmholtz-Institut für Strahlen und Kernphysik, Bonn, Germany*

¹⁸*Fakultät Physik, Technische Universität Dortmund, Dortmund, Germany*

¹⁹*Max-Planck-Institut für Kernphysik (MPIK), Heidelberg, Germany*

²⁰*Physikalisches Institut, Ruprecht-Karls-Universität Heidelberg, Heidelberg, Germany*

²¹*School of Physics, University College Dublin, Dublin, Ireland*

²²*INFN Sezione di Bari, Bari, Italy*

²³*INFN Sezione di Bologna, Bologna, Italy*

- ²⁴ INFN Sezione di Ferrara, Ferrara, Italy
- ²⁵ INFN Sezione di Firenze, Firenze, Italy
- ²⁶ INFN Laboratori Nazionali di Frascati, Frascati, Italy
- ²⁷ INFN Sezione di Genova, Genova, Italy
- ²⁸ INFN Sezione di Milano, Milano, Italy
- ²⁹ INFN Sezione di Milano-Bicocca, Milano, Italy
- ³⁰ INFN Sezione di Cagliari, Monserrato, Italy
- ³¹ INFN Sezione di Padova, Padova, Italy
- ³² INFN Sezione di Perugia, Perugia, Italy
- ³³ INFN Sezione di Pisa, Pisa, Italy
- ³⁴ INFN Sezione di Roma La Sapienza, Roma, Italy
- ³⁵ INFN Sezione di Roma Tor Vergata, Roma, Italy
- ³⁶ Nikhef National Institute for Subatomic Physics, Amsterdam, Netherlands
- ³⁷ Nikhef National Institute for Subatomic Physics and VU University Amsterdam, Amsterdam, Netherlands
- ³⁸ AGH - University of Krakow, Faculty of Physics and Applied Computer Science, Kraków, Poland
- ³⁹ Henryk Niewodniczanski Institute of Nuclear Physics Polish Academy of Sciences, Kraków, Poland
- ⁴⁰ National Center for Nuclear Research (NCBJ), Warsaw, Poland
- ⁴¹ Horia Hulubei National Institute of Physics and Nuclear Engineering, Bucharest-Magurele, Romania
- ⁴² Authors affiliated with an institute formerly covered by a cooperation agreement with CERN
- ⁴³ DS4DS, La Salle, Universitat Ramon Llull, Barcelona, Spain
- ⁴⁴ ICCUB, Universitat de Barcelona, Barcelona, Spain
- ⁴⁵ Instituto Galego de Física de Altas Enerxías (IGFAE), Universidade de Santiago de Compostela, Santiago de Compostela, Spain
- ⁴⁶ Instituto de Física Corpuscular, Centro Mixto Universidad de Valencia - CSIC, Valencia, Spain
- ⁴⁷ European Organization for Nuclear Research (CERN), Geneva, Switzerland
- ⁴⁸ Institute of Physics, Ecole Polytechnique Fédérale de Lausanne (EPFL), Lausanne, Switzerland
- ⁴⁹ Physik-Institut, Universität Zürich, Zürich, Switzerland
- ⁵⁰ NSC Kharkiv Institute of Physics and Technology (NSC KIPT), Kharkiv, Ukraine
- ⁵¹ Institute for Nuclear Research of the National Academy of Sciences (KINR), Kyiv, Ukraine
- ⁵² School of Physics and Astronomy, University of Birmingham, Birmingham, United Kingdom
- ⁵³ H.H. Wills Physics Laboratory, University of Bristol, Bristol, United Kingdom
- ⁵⁴ Cavendish Laboratory, University of Cambridge, Cambridge, United Kingdom
- ⁵⁵ Department of Physics, University of Warwick, Coventry, United Kingdom
- ⁵⁶ STFC Rutherford Appleton Laboratory, Didcot, United Kingdom
- ⁵⁷ School of Physics and Astronomy, University of Edinburgh, Edinburgh, United Kingdom
- ⁵⁸ School of Physics and Astronomy, University of Glasgow, Glasgow, United Kingdom
- ⁵⁹ Oliver Lodge Laboratory, University of Liverpool, Liverpool, United Kingdom
- ⁶⁰ Imperial College London, London, United Kingdom
- ⁶¹ Department of Physics and Astronomy, University of Manchester, Manchester, United Kingdom
- ⁶² Department of Physics, University of Oxford, Oxford, United Kingdom
- ⁶³ Massachusetts Institute of Technology, Cambridge, MA, United States
- ⁶⁴ University of Cincinnati, Cincinnati, OH, United States
- ⁶⁵ University of Maryland, College Park, MD, United States
- ⁶⁶ Los Alamos National Laboratory (LANL), Los Alamos, NM, United States
- ⁶⁷ Syracuse University, Syracuse, NY, United States
- ⁶⁸ Pontifícia Universidade Católica do Rio de Janeiro (PUC-Rio), Rio de Janeiro, Brazil, associated to ³
- ⁶⁹ School of Physics and Electronics, Hunan University, Changsha City, China, associated to ⁸
- ⁷⁰ Guangdong Provincial Key Laboratory of Nuclear Science, Guangdong-Hong Kong Joint Laboratory of Quantum Matter, Institute of Quantum Matter, South China Normal University, Guangzhou, China, associated to ⁴
- ⁷¹ Lanzhou University, Lanzhou, China, associated to ⁵
- ⁷² School of Physics and Technology, Wuhan University, Wuhan, China, associated to ⁴
- ⁷³ Departamento de Física, Universidad Nacional de Colombia, Bogota, Colombia, associated to ¹⁵
- ⁷⁴ Ruhr Universitaet Bochum, Fakultae f. Physik und Astronomie, Bochum, Germany, associated to ¹⁸
- ⁷⁵ Eotvos Lorand University, Budapest, Hungary, associated to ⁴⁷

- ⁷⁶ *Van Swinderen Institute, University of Groningen, Groningen, Netherlands, associated to* ³⁶
⁷⁷ *Universiteit Maastricht, Maastricht, Netherlands, associated to* ³⁶
⁷⁸ *Tadeusz Kosciuszko Cracow University of Technology, Cracow, Poland, associated to* ³⁹
⁷⁹ *Universidade da Coruña, A Coruña, Spain, associated to* ⁴³
⁸⁰ *Department of Physics and Astronomy, Uppsala University, Uppsala, Sweden, associated to* ⁵⁸
⁸¹ *University of Michigan, Ann Arbor, MI, United States, associated to* ⁶⁷
⁸² *Université Paris-Saclay, Centre d'Etudes de Saclay (CEA), IRFU, Saclay, France, Gif-Sur-Yvette, France*

^a *Universidade de Brasília, Brasília, Brazil*

^b *Centro Federal de Educação Tecnológica Celso Suckow da Fonseca, Rio De Janeiro, Brazil*

^c *Center for High Energy Physics, Tsinghua University, Beijing, China*

^d *Hangzhou Institute for Advanced Study, UCAS, Hangzhou, China*

^e *School of Physics and Electronics, Henan University, Kaifeng, China*

^f *LIP6, Sorbonne Université, Paris, France*

^g *Lamarr Institute for Machine Learning and Artificial Intelligence, Dortmund, Germany*

^h *Universidad Nacional Autónoma de Honduras, Tegucigalpa, Honduras*

ⁱ *Università di Bari, Bari, Italy*

^j *Università di Bergamo, Bergamo, Italy*

^k *Università di Bologna, Bologna, Italy*

^l *Università di Cagliari, Cagliari, Italy*

^m *Università di Ferrara, Ferrara, Italy*

ⁿ *Università di Genova, Genova, Italy*

^o *Università degli Studi di Milano, Milano, Italy*

^p *Università degli Studi di Milano-Bicocca, Milano, Italy*

^q *Università di Padova, Padova, Italy*

^r *Università di Perugia, Perugia, Italy*

^s *Scuola Normale Superiore, Pisa, Italy*

^t *Università di Pisa, Pisa, Italy*

^u *Università della Basilicata, Potenza, Italy*

^v *Università di Roma Tor Vergata, Roma, Italy*

^w *Università di Siena, Siena, Italy*

^x *Università di Urbino, Urbino, Italy*

^y *Universidad de Alcalá, Alcalá de Henares, Spain*

^z *Facultad de Ciencias Físicas, Madrid, Spain*

^{aa} *Department of Physics/Division of Particle Physics, Lund, Sweden*

[†] *Deceased*